



BRAHMA-interacting proteins BRIP1 and BRIP2 are core subunits of *Arabidopsis* SWI/SNF complexes

Yaoguang Yu¹, Zhenwei Liang¹, Xin Song¹, Wei Fu¹, Jianqu Xu¹, Yawen Lei¹, Liangbing Yuan¹, Jiuxiao Ruan¹, Chen Chen², Wenqun Fu³, Yuhai Cui², Shangzhi Huang¹ and Chenlong Li¹✉

Switch defective/sucrose non-fermentable (SWI/SNF) chromatin remodelling complexes are multi-protein machineries that control gene expression by regulating chromatin structure in eukaryotes. However, the full subunit composition of SWI/SNF complexes in plants remains unclear. Here we report that in *Arabidopsis thaliana*, two homologous glioma tumour suppressor candidate region domain-containing proteins, named BRAHMA-interacting proteins1 (BRIP1) and BRIP2, are core subunits of plant SWI/SNF complexes. *brip1 brip2* double mutants exhibit developmental phenotypes and a transcriptome remarkably similar to those of BRAHMA (BRM) mutants. Genetic interaction tests indicated that BRIP1 and BRIP2 act together with BRM to regulate gene expression. Furthermore, BRIP1 and BRIP2 physically interact with BRM-containing SWI/SNF complexes and extensively co-localize with BRM on chromatin. Simultaneous mutation of BRIP1 and BRIP2 results in decreased BRM occupancy at almost all BRM target loci and substantially reduced abundance of the SWI/SNF assemblies. Together, our work identifies new core subunits of BRM-containing SWI/SNF complexes in plants and uncovers the essential role of these subunits in maintaining the abundance of SWI/SNF complexes in plants.

Switch defective/sucrose non-fermentable (SWI/SNF) complexes are essential in the regulation of gene expression through modulation of chromatin architecture^{1–5}. They use energy derived from ATP hydrolysis to destabilize the interactions between DNA and histones to translocate, evict or change the composition of nucleosomes³. SWI/SNF complexes are multi-protein machineries evolutionarily conserved among yeasts, animals and plants^{5,6}. Yeast SWI/SNF complexes are composed of eight to 14 subunits while mammalian SWI/SNF complexes are assembled from the products of 29 genes, including multiple paralogues^{1–3}. Genetic experiments in the flowering plant *Arabidopsis thaliana* have revealed several core subunits of plant SWI/SNF complexes, including four SWI2/SNF2 ATPases (BRAHMA (BRM), SPLAYED (SYD), chromatin remodeling 12 (CHR12) and 23 (CHR23)); four SWI3 proteins (SWI3A–SWI3D); two SWI/SNF associated proteins 73 (SWP73A and SWP73B); two actin-related proteins (ARP4 and ARP7); and a single SNF5 subunit termed BUSHY (BSH)^{6–8}. Although canonical plant SWI/SNF complexes were thought to contain one ATPase, two SWI3 subunits, one SWP73 and one SNF5 subunit⁷, several studies have implicated the existence of potential new subunits of SWI/SNF complexes in plants^{9–11}. However, the full subunit composition of SWI/SNF complexes in plants remains unclear.

BRAHMA is one of the ATPase subunits of SWI/SNF complexes that is pivotal for plant development and responses to environments, through regulation of the transcription of relevant target genes^{6,7,11–20}. The loss of function of BRM causes pleiotropic phenotypes, suggesting diverse functions of this protein in plant development. BRM was reported to be essential in the regulation of leaf development, root stem cell maintenance, flower patterning,

flowering time, embryo development, the transition from vegetative to adult phase^{9,12,13,18,19,21–24} as well as heat stress memory and hormonal responses^{6,25}. Other core subunits of plant SWI/SNF complexes, such as SWI3 and SWP73 proteins, have also been reported to be involved in many of the processes regulated by BRM^{26–31}. In *Arabidopsis* seedlings, BRM occupies thousands of genes¹¹ and regulation of some of these target genes at the transcriptional level by BRM has been shown to be responsible for the phenotypes of *brm* mutants^{7,12,13,15,21,22}. We previously showed that the occupancy of BRM at a subset of its target genes is dependent on the plant-unique H3K27me3 demethylase RELATIVE OF EARLY FLOWERING6 (REF6)¹¹. In addition, BRM can also be recruited to chromatin by different transcription factors^{9,18,22–24}. Although the biological functions of several subunits of SWI/SNF complexes in plant growth, development and stress responses have been studied extensively^{6,7,14}, the roles of most subunits in assembly, as well as targeting, of the complexes remain largely unknown.

Here, we show that *Arabidopsis* BRM-interacting proteins1 (BRIP1) and BRIP2, two homologous glioma tumour suppressor candidate region (GLTSCR) domain-containing proteins, are core subunits of plant SWI/SNF complexes. We found that *brip1 brip2* double mutants display developmental phenotypes remarkably similar to those of *brm* mutants. Genetic interaction tests and transcriptome analysis indicated that BRIP1 and 2 act in the same pathways with BRM to regulate gene expression. BRIP1 and 2 physically interact with BRM-containing SWI/SNF complexes and extensively co-localize with BRM on chromatin. Finally, we demonstrate that BRIP1/BRIP2 function to maintain protein levels of members of the BRM-containing SWI/SNF complexes, enabling their proper assembly and association with chromatin.

¹State Key Laboratory of Biocontrol, Guangdong Provincial Key Laboratory of Plant Resources, School of Life Sciences, Sun Yat-Sen University, Guangzhou, China. ²London Research and Development Centre, Agriculture and Agri-Food Canada, London, Ontario, Canada. ³School of Biological Science and Biotechnology, Minnan Normal University, Zhangzhou, China. ✉e-mail: lichlong3@mail.sysu.edu.cn

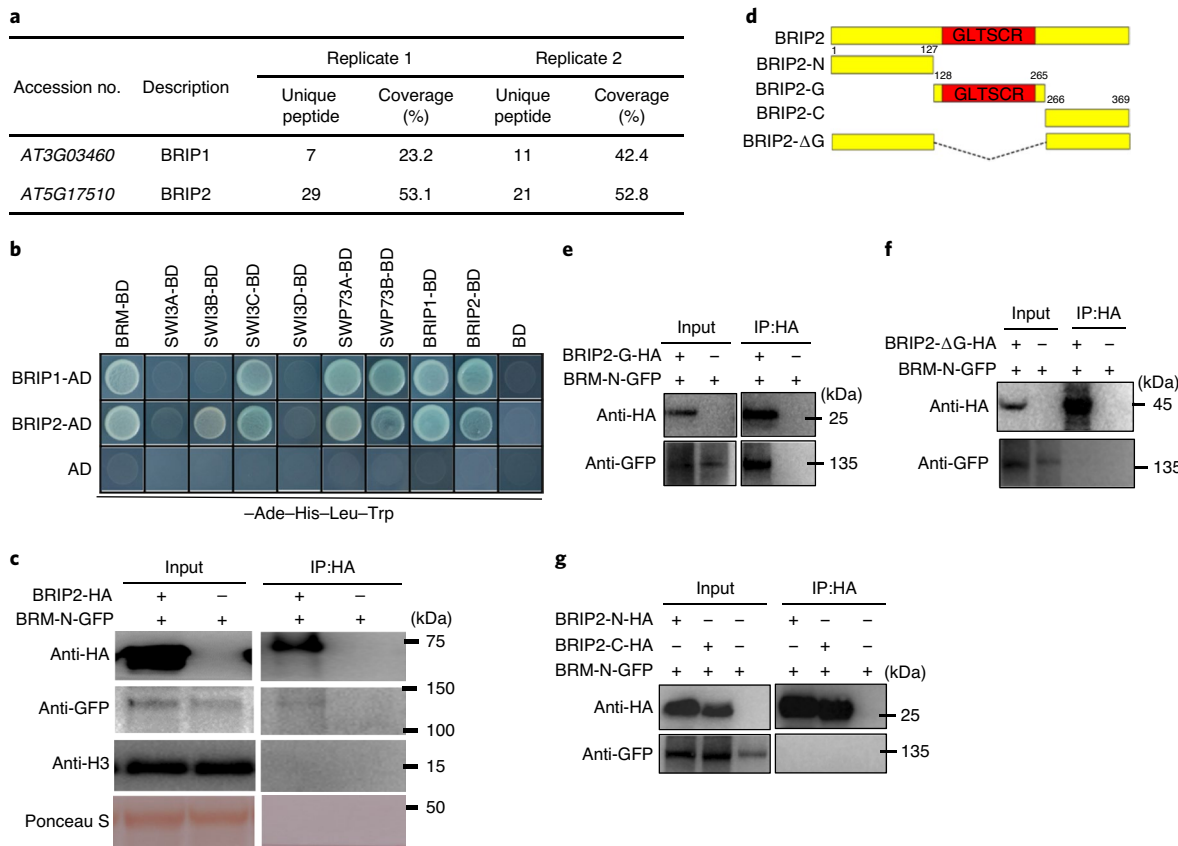


Fig. 1 | BRIP1 and BRIP2 interact with BRM-containing SWI/SNF complexes. **a**, Summary of the peptides of BRIP1 and BRIP2 identified by mass spectrometry from an anti-GFP purification of a BRM-GFP stably expressed line. Two biological replicates are shown. **b**, Y2H assay to examine the direct interaction among BRIP1, BRIP2 and members of SWI/SNF complexes. Growth of transformed yeast is shown on permissive SD-Ade-His-Leu-Trp medium. **c**, Co-immunoprecipitation of BRIP2 with BRM-N (N-terminal of BRM, amino acids 1–952). BRM-N-GFP was immunoprecipitated with an anti-HA-agarose antibody from protoplasts co-transfected with BRM-N-GFP and BRIP2-HA. H3 (histone 3) and Ponceau S staining are shown as loading controls. **d**, Schematic illustration of the BRIP2 protein and its truncated versions. **e–g**, Co-immunoprecipitation of different truncations of BRIP2 with BRM-N. Immunoprecipitation was performed with an anti-HA-agarose antibody using tobacco leaves co-transfected with BRM-N-GFP and BRIP2-ΔG-HA (**f**), BRIP2-G-HA (**e**), and BRIP2-N-HA or BRIP2-C-HA (**g**). For immunoblotting, the antibodies used are indicated on the left and the sizes of the protein markers are indicated on the right.

Results

BRIP1 and BRIP2 interact with BRM-containing SWI/SNF complexes in plants. To search for novel proteins that might play a role in the regulation of BRM targeting, we performed immunoprecipitation using a transgenic line stably expressing green fluorescent protein (GFP)-tagged BRM in the *brm-1* null mutant background¹², and identified proteins that co-purified with BRM by mass spectrometry¹¹. In addition to known plant SWI/SNF core members, including SWI3A, SWI3B, SWI3C, SWI3D, SWP73A and SWP73B¹¹, this analysis isolated two previously uncharacterized proteins, which we named BRIP1 and BRIP2, that are encoded by *AT3G03460* and *AT5G17510*, respectively (Fig. 1a). They were selected as candidates for core subunits of plant SWI/SNF complexes because both the number and coverage of unique peptides corresponding to the two proteins were comparable to those of established plant SWI/SNF complex subunits (Supplementary Table 1).

We confirmed the physical interaction between BRIP1/2 and plant SWI/SNF complexes through several independent assays. In yeast two-hybrid (Y2H) assays, we found that both BRIP1 and BRIP2 interacted with BRM (Fig. 1b). Furthermore, bimolecular fluorescence complementation (BiFC) analyses, in which BRIP1 or BRIP2 was fused to N-terminal YFP, whereas BRM was fused to the C-terminal YFP, showed that BRIP1 and BRIP2 interacted with

BRM in the nucleus (Extended Data Fig. 1a). No signal was observed when an unrelated nuclear-localized protein³² was used (Extended Data Fig. 1a). Finally, we performed co-immunoprecipitation (co-IP) and observed that haemagglutinin (HA)-tagged BRIP1 or BRIP2 precipitated GFP-tagged BRM in *Arabidopsis* (Fig. 1c and Extended Data Fig. 1b).

Further deletion analysis in yeast showed that the N-terminal part of BRM (amino acids 1–952) was responsible for the interaction with BRIP1 or BRIP2 (Extended Data Fig. 1c). The N-terminal region of BRM has been shown to mediate the protein–protein interaction of BRM with numerous proteins^{18,24,33,34}. Both BRIP1 and BRIP2 contain a GLTSCR domain (Fig. 1d). To map the region of BRIP2 that is responsible for interaction with BRM, we made constructs encoding truncated versions of BRIP2—that is, N-terminal (BRIP2-N), GLTSCR domain (BRIP2-G), C-terminal (BRIP2-C) and GLTSCR domain-deleted (BRIP2-ΔG) (Fig. 1d)—and used them for co-IP. The co-IP assays showed that the GLTSCR domain of BRIP2 (BRIP2-G) was enough to form complexes with BRM in plants (Fig. 1e), while deletion of the GLTSCR domain (BRIP2-ΔG) abolished the interaction (Fig. 1f). In addition, the N-terminal (BRIP2-N) and C-terminal (BRIP2-C) portions were unable to interact with BRM (Fig. 1g). These results suggest that the GLTSCR domain is required and sufficient for the interaction of BRIP2 with BRM in planta.

Among the four SWI3 proteins, SWI3B and SWI3C, but not SWI3A and SWI3D, are considered to be the core subunits of BRM-containing SWI/SNF complexes, based on their direct interaction with BRM and the similar loss-of-function phenotypes of *swi3c* and *brm* mutants³⁴. We found that BRIP1 interacted with SWI3C, while BRIP2 interacted with SWI3B and SWI3C in yeast (Fig. 1b). Neither BRIP1 nor BRIP2 interacted with SWI3A and SWI3D (Fig. 1b). BiFC assays confirmed that BRIP1 interacted with SWI3C, and BRIP2 interacted with SWI3B and SWI3C in the nucleus (Extended Data Fig. 1a). Both BRIP1 and BRIP2 also interacted with SWP73A and SWP73B (Fig. 1b and Extended Data Fig. 1a). Notably, BRIP1 and BRIP2 can also interact with each other or itself (Fig. 1b and Extended Data Fig. 1a). Together, these data suggest that BRIP1 and BRIP2 are part of BRM-containing SWI/SNF complexes.

***brrip1 brrip2* double mutants show phenotypes similar to *brm*.**

Next, we determined whether BRIP1 and BRIP2 share common biological functions with BRM. Analysis of the amino acid sequences of BRIP1 and BRIP2 showed that the two proteins have high homology (Extended Data Fig. 2a). The β -GLUCURONIDASE (GUS) reporter gene driven by the promoter of either *BRIP1* or *BRIP2* showed that the two genes had similar temporal and spatial expression patterns (Supplementary Fig. 1). These observations suggested that BRIP1 and BRIP2 might have redundant functions. We obtained transfer DNA insertion mutants for each of the *BRIP* genes (*brrip1-1* and *brrip2-1*) (Extended Data Fig. 2b,c) and generated *brrip1 brrip2* double mutants. Quantitative PCR with reverse transcription (RT-qPCR) data in the two single mutants confirmed the disruption of the corresponding transcripts and demonstrated that there were no compensatory gene expression effects observed between BRIP1 and BRIP2 (Extended Data Fig. 2d).

We then examined phenotypes of the *brrip* mutants and compared them with those of *brm* mutants. Typical phenotypes associated with mutations of BRM ATPase include small, downward-curled leaves, precocious flowering and reduced embryo fertility^{12,15,16}. Although the leaf morphology of neither *brrip1* nor *brrip2* single mutants was different from wild-type (WT) controls, the leaves of *brrip1 brrip2* double mutants were downward curled (Fig. 2a and Extended Data Fig. 3a). Furthermore, the *brrip1 brrip2* double mutants flowered earlier than WT under long-day conditions and had shortened siliques (Extended Data Fig. 3c,d), whereas the *brrip1* and *brrip2* single mutants developed normally except for a moderate early flowering of the latter. These phenotypes in the *brrip1 brrip2* double mutants are reminiscent of *brm* mutants and indicate that BRIP1 and BRIP2 function in substantial redundancy. GFP-tagged BRIP1 or BRIP2 expressed under their corresponding native promoter complemented the *brrip1 brrip2* double mutant phenotypes (Fig. 2a and Extended Data Fig. 3b).

Hypomorphic mutant phenotypes can be enhanced by loss-of-function mutations in genes that act in the same pathway³⁵. We crossed *brrip1 brrip2* with the hypomorphic *brm-3* allele to assess whether BRIP1/2 and BRM act in the same pathways. The triple mutants of *brrip1 brrip2* and the weak *brm-3* allele had leaves with more severe downward curling than either parent (Fig. 2a). Therefore, *brrip1 brrip2* enhanced the leaf-curling phenotype of the *brm-3* mutant. In contrast, the triple mutants of *brrip1 brrip2* and the null *brm-1* allele showed the same leaf curling, flowering time and siliques length phenotypes as *brm-1* (Fig. 2a and Extended Data Fig. 3c,d). Thus, *brrip1 brrip2* did not enhance the phenotypes of null *brm-1* mutants. These combined data demonstrate that BRIP1 and BRIP2 are essential for plant development and support the notion that BRIP1/2 and BRM are in the same complexes for the regulation of plant development.

BRIP1/2 and BRM co-regulate gene expression genome-wide.

We performed RNA-sequencing (RNA-seq) and compared the

transcriptome data of *brrip1 brrip2* with those of mutants *brm* (*brm-3* and *brm-1*) and *brrip1 brrip2 brm-1* (Extended Data Fig. 4a and Supplementary Table 2). The transcriptome profile observed in *brrip1 brrip2* double mutants was very similar to that of *brm* mutants (Fig. 2b-d and Extended Data Fig. 4b,c), consistent with the similar phenotypes of mutants *brrip1 brrip2* and *brm*. Approximately 80% of the 447 upregulated and 460 downregulated genes in *brrip1 brrip2* (336 and 377, respectively) exhibited the same direction of misregulation in *brm-1* mutants (Fig. 2b). A high overlap was also observed between *brrip1 brrip2* and *brm-3* (Extended Data Fig. 4b). The transcriptome of *brrip1 brrip2* was strongly positively correlated with that of mutants *brm-1* (correlation coefficient = 0.844; Fig. 2c) or *brm-3* (correlation coefficient = 0.837; Extended Data Fig. 4c). In contrast, the transcriptome profiles of *brrip1* and *brrip2* single mutants clustered separately (Fig. 2d,e), and changes in the *brrip1* or *brrip2* single mutants and *brm-1* were not correlated (Extended Data Fig. 4c). Moreover, the transcriptome of *brrip1 brrip2 brm-1* triple mutants was extremely positively correlated with that of *brm-1* (correlation coefficient = 0.905; Extended Data Fig. 4c). Together, these data show that BRIP1/2 and BRM act together extensively to regulate gene expression in *Arabidopsis*. Gene Ontology (GO) analysis showed that GO terms such as plant hormone responses and decreased oxygen levels were commonly over-represented for upregulated genes in *brm-1*, *brrip1 brrip2* and *brm-1 brrip1 brrip2*, whereas downregulated genes were enriched for terms such as secondary metabolic process (Supplementary Fig. 2).

BRIP1/2 co-occupy with BRM genome-wide. Because the data so far suggest that BRIP1/2 interact with BRM-containing SWI/SNF complexes and that loss of BRIP1/2 leads to phenotypes and transcriptome changes similar to *brm* mutants, we assessed whether BRIP1/2 co-localize with BRM-containing SWI/SNF complexes in the *Arabidopsis* genome. We determined BRIP1 and BRIP2 genome-wide occupancy via chromatin immunoprecipitation-sequencing (ChIP-seq) experiments using plants expressing GFP-tagged BRIP1 or BRIP2 in their respective single mutant background (Extended Data Fig. 5). The BRIP1-GFP and BRIP2-GFP transgenes are functional in vivo because either could complement the phenotypes of *brrip1 brrip2* (Fig. 2a). Meanwhile, we also determined the genome-wide occupancy of BRM using the previously generated GFP-tagged BRM line (BRM-GFP)¹². Through ChIP-seq analyses, we identified 5,035 BRIP1 target loci and 7,023 BRIP2 target loci in *Arabidopsis* seedlings (Supplementary Table 3). Eighty-nine per cent of the BRIP1 targets (4,501 sites) were also occupied by BRIP2 (Fig. 3a,c), consistent with the functional redundancy of the two proteins.

The ChIP-seq analyses showed that BRIP1, BRIP2 and BRM had highly comparable occupancy profiles at target loci (Fig. 3). The distribution of BRIP1, BRIP2 and BRM over genes was very similar (Extended Data Fig. 6a), and the majority of BRIP1 or BRIP2 occupancy peaks were enriched in the gene body proximal to the transcription start site (TSS), similar to BRM (Extended Data Fig. 6b). In total, 52% (4,026/7,767) and 73% (5,644/7,767) of BRM targets were co-occupied by BRIP1 and BRIP2, respectively (Fig. 3a-c). BRIP1 and BRIP2 displayed strong enrichment right over the summits of BRM-occupied sites (Fig. 3d). ChIP-seq data showing the co-localization of BRIP1, BRIP2 and BRM at selected loci are presented in Fig. 3e, and were validated by independent ChIP-qPCR (Fig. 3f). Basic GO analysis showed very similar distribution patterns of BRIP1/2 and BRM in GO biological process (Extended Data Fig. 6c). The BRIP1/2 and BRM co-occupied genes also presented similar GO distribution (Extended Data Fig. 6c), suggesting that the general function of BRIP1/2 targeted genes and BRM targeted genes may be very similar. Notably, the BRM target genes that were up- or downregulated in *brm-1* had a strong overlap with those in *brrip1 brrip2* (Supplementary Fig. 3). Moreover,

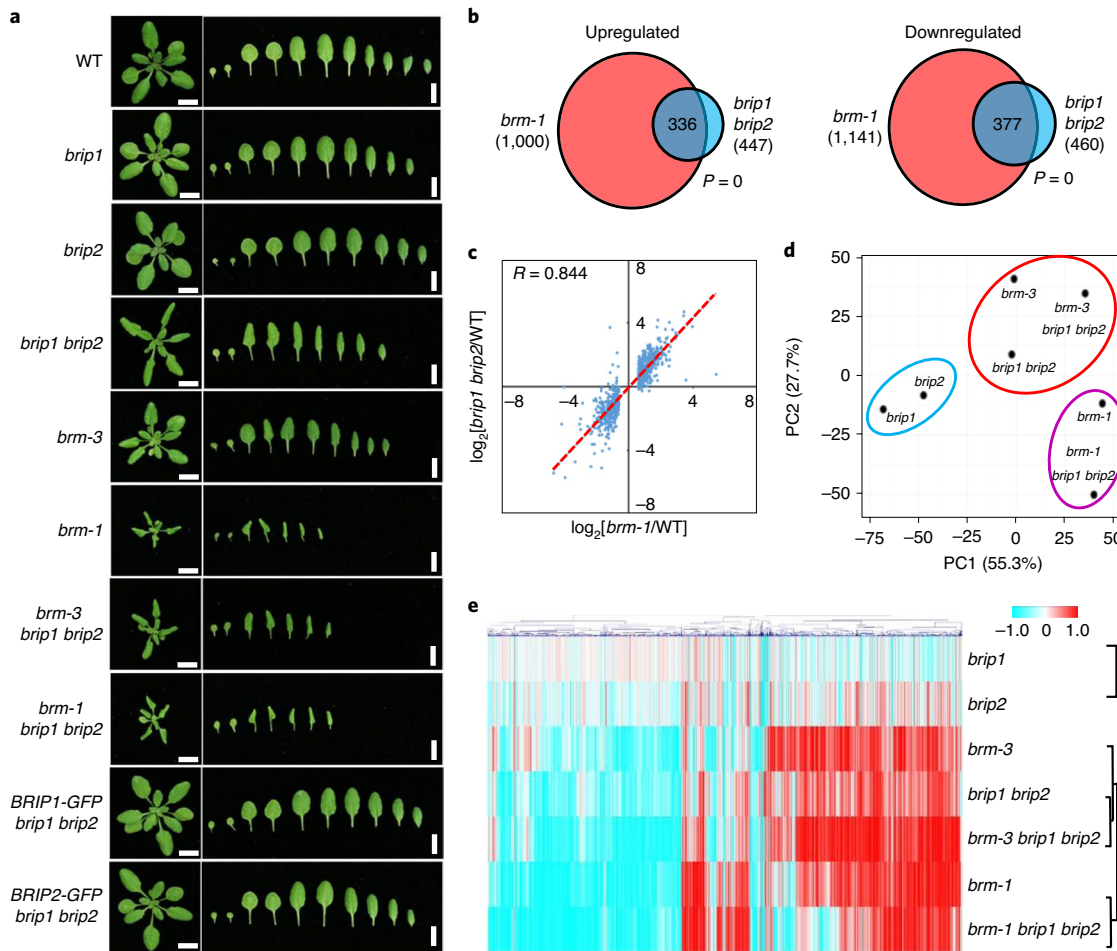


Fig. 2 | *brip1 brip2* double mutants show phenotypes similar to *brm*. **a**, Leaf phenotype of 21-day-old seedlings. Scale bars, 1 cm. **b**, Venn diagrams showing statistically significant overlaps between genes up- or downregulated in *brm-1* and those in *brip1 brip2*. $P=0$, hypergeometric test. **c**, Scatterplot of \log_2 -fold change values over WT of *brm-1* versus *brip1 brip2* at genes that were differentially expressed in *brm-1*. Line of best fit is shown in red, with adjusted R value indicated. Dots are mean values from three biologically independent experiments. **d**, PCA of *brip1*, *brip2*, *brm-3*, *brm-1*, *brip1 brip2*, *brm-3 brip1 brip2* and *brm-1 brip1 brip2*. Percentages represent variance captured by PC1 and PC2 in each analysis. Clustering groups are represented by different colours. **e**, Heat map showing hierarchical clustering of differentially expressed genes in different mutants. Red and blue represent up- and downregulation in mutants, respectively (total misregulated genes, 3,455).

the expression changes of BRM target genes in the *brm-1* mutant showed a strong positive correlation with those in *brip1 brip2* mutants (correlation coefficient = 0.86; Fig. 3g), consistent with the model that BRIP1 and BRIP2 form complexes with BRM to regulate gene expression in *Arabidopsis*. In sum, direct interaction between BRIP1/2 and BRM, their co-occupancy across the *Arabidopsis* genome and similar mutant phenotypes and transcriptome changes strongly suggest that BRIP1 and BRIP2 are integral (dedicated) sub-units of BRM-containing SWI/SNF complexes in plants.

BRIP1 and BRIP2 are required for the binding of BRM to target genes genome-wide. To address whether BRIP1 and BRIP2 are redundantly required for the occupancy of BRM to target genes, we compared the genome-wide occupancy of BRM in WT with that in *brip1 brip2* by ChIP-seq. The numbers of BRM-associated peaks and corresponding genes were obviously decreased in *brip1 brip2* compared to WT (Fig. 4a). Furthermore, >90% of BRM binding sites showed a marked reduction in, or elimination of, BRM occupancy in the absence of BRIP1 and 2, while only 20 loci showed an increase (Fig. 4b). The average occupancy intensity of BRM was substantially reduced in *brip1 brip2*, both globally (Fig. 4c) and at individual loci (Fig. 4d). Independent ChIP-qPCR confirmed

the reduction of BRM occupancy at individual loci in *brip1 brip2* (Fig. 4e). Thus, the association of BRM with chromatin is largely dependent on BRIP1/2. Interestingly, the occupancy of BRIP1 and BRIP2 at target genes was also obviously decreased in the *brm-1* mutant, indicating that BRM is required for the association of BRIP1/2 with chromatin (Extended Data Fig. 7).

BRIP1 and BRIP2 are required for maintaining the abundance of SWI/SNF complexes. The absence of a distinct DNA binding domain in BRIP1 or BRIP2 argues against a function for them in recruitment of BRM by direct binding to target genes. We thus reasoned that BRIP1 and BRIP2 might be necessary for the construction of BRM-containing SWI/SNF complexes. The loss of BRIP1/2 did not significantly change the messenger RNA levels of *BRM-GFP* (Fig. 5a), but resulted in substantially reduced protein levels of BRM-GFP (Fig. 5b,c). Treatment with the proteasome inhibitor MG132 increased the protein levels of BRM-GFP in *brip1 brip2* (Fig. 5d), suggesting that the observed reduction in protein levels was probably the result of post-translational regulation. Furthermore, immunoprecipitation of FLAG-tagged SWI3C (SWI3C-FLAG) or BRM-GFP followed by mass spectrometry analysis showed that mutations of BRIP1/2 resulted in significantly

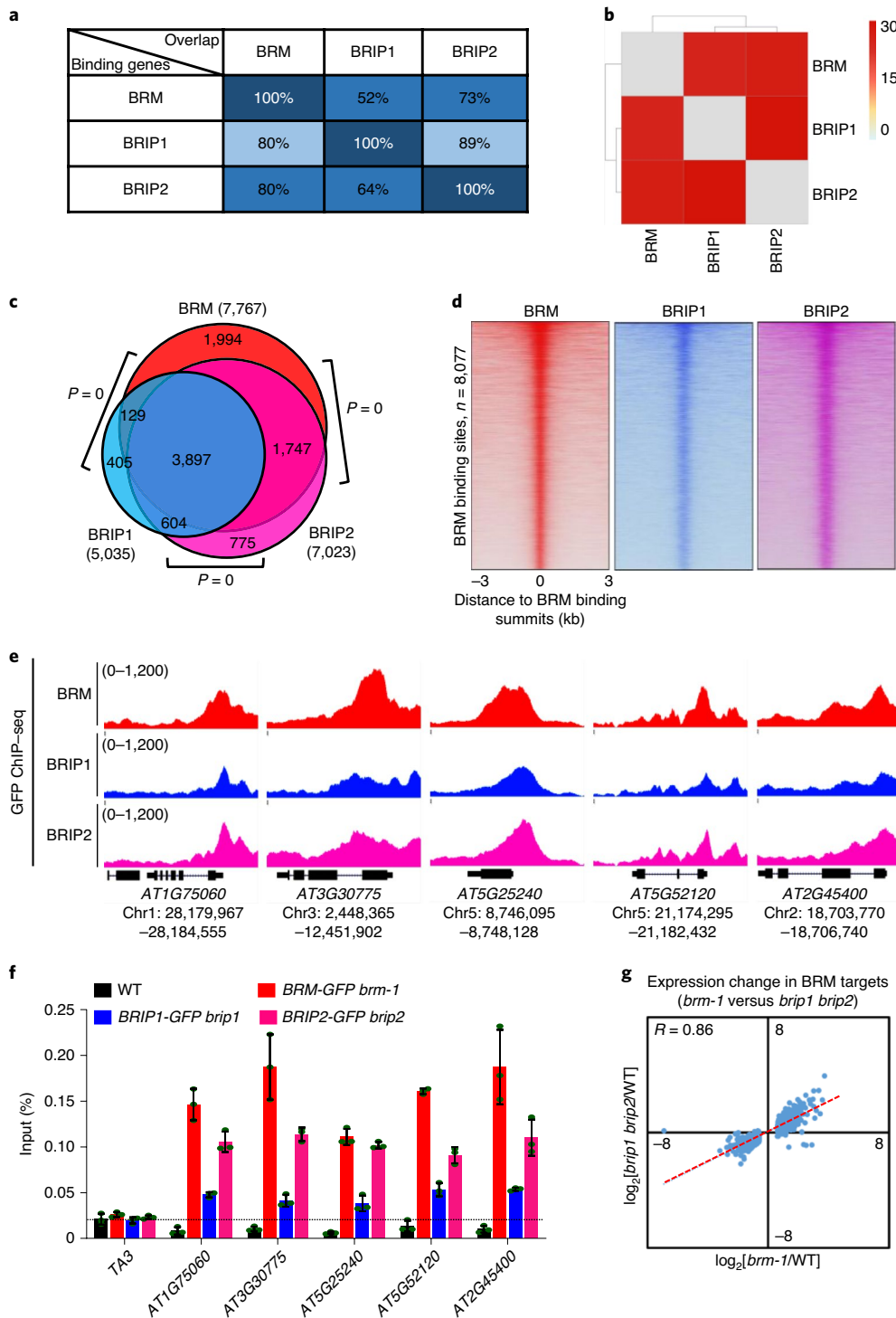


Fig. 3 | BRIP1 and BRIP2 co-occupy with BRM genome-wide. **a**, Percentages of BRM, BRIP1 and BRIP2 binding genes (by row) overlapping with other binding genes (by column). Shading indicates the strength of overlap. **b**, Mutual overlap among BRM, BRIP1 and BRIP2 peaks. $P = 0$, significance was tested by permutation ($n=100$)⁷⁹. Heat map shows enrichment scores: $Z = \log_2 \frac{\text{observed overlap}}{\text{expected overlap}}$ ($-\log_{10}[P\text{ value}]$). **c**, Venn diagrams displaying statistically significant overlaps between genes occupied by BRM, BRIP1 and BRIP2. The numbers in brackets indicate the total number of genes occupied by BRM, BRIP1 or BRIP2. Hypergeometric test. **d**, Heat map representation of the co-occupancy of BRM, BRIP1 and BRIP2 in the genome. The horizontal lines represent individual BRM-bound regions (left), BRIP1-bound regions (middle) or BRIP2-bound regions (right). The binding intensity is indicated by colour shading. **e**, IGV views of ChIP-seq signals on representative genes in *BRM-GFP brm-1*, *BRIP1-GFP bripl* and *BRIP2-GFP bripl*. The scale is identical for the different tracks, and the black diagrams indicate gene structure and ID. The y-axis scales represent shifted merged MACS2 tag counts for every 10-bp window. **f**, Validation of ChIP-seq signals at five different genomic loci by ChIP-qPCR in WT, *BRM-GFP brm-1*, *BRIP1-GFP bripl* and *BRIP2-GFP bripl*. TA3 serves as a negative control. Mean \pm s.d.; three biological replicates are included. **g**, Scatterplot of \log_2 fragments per kilobase exon per million mapped reads fold change over WT of *brm-1* versus *brip1 bripl* at BRM direct target genes that were differentially expressed in *brm-1*. Line of best fit is shown in red, with adjusted R indicated. Dots are mean values from three biologically independent experiments.

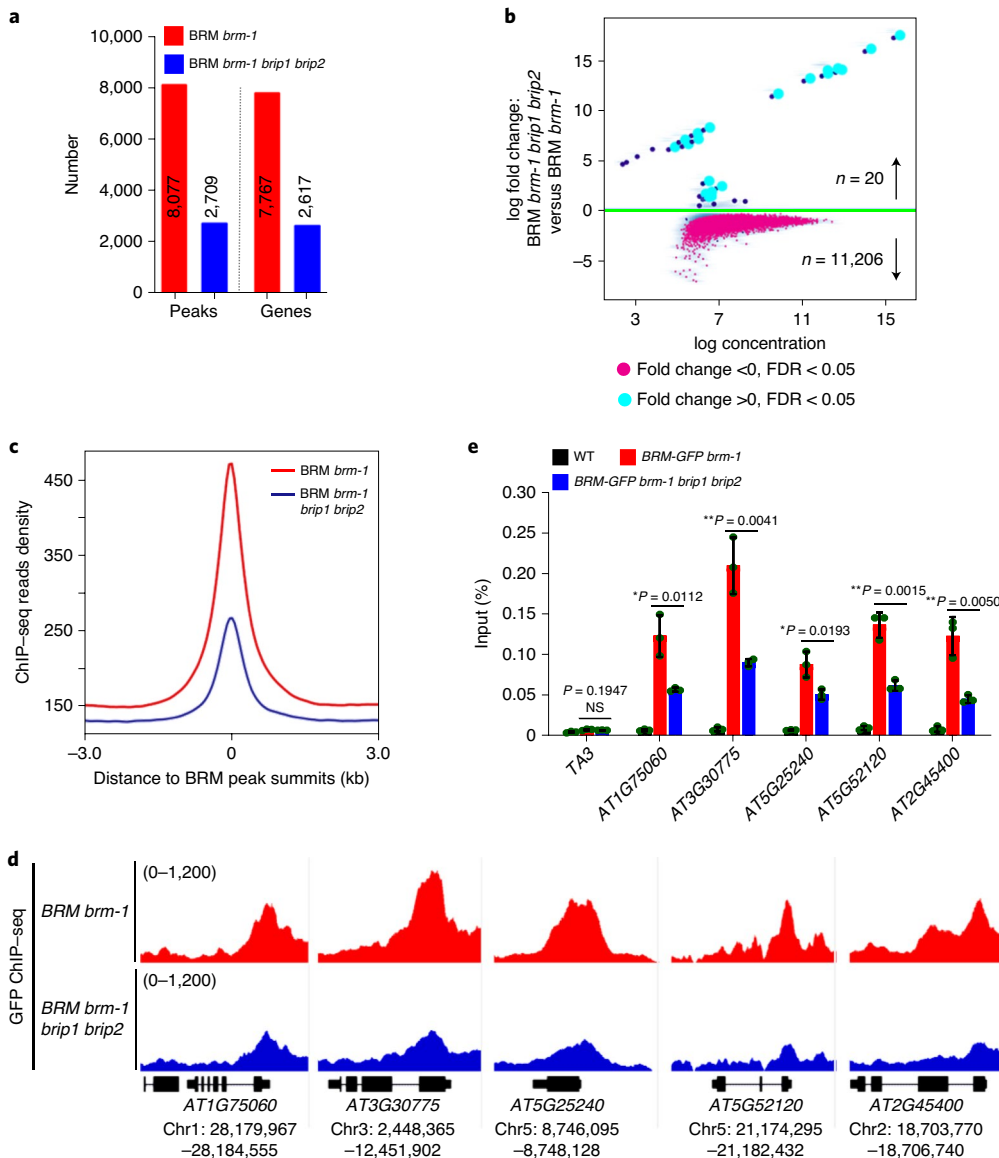


Fig. 4 | Loss of BRIP1/2 leads to genome-wide decrease in BRM occupancy. **a**, Number of BRM binding sites (number of peaks or genes) in the WT and *brip1 brip2* background. **b**, Fold change (\log_2) in BRM occupancy between WT and *brip1 brip2* background. Occupancy changes with false discovery rate (FDR) < 0.05 are highlighted; the 20 peaks with fold change > 0 are enlarged and marked in sky blue; pink dots indicate 11,206 peaks with decreased BRM occupancy in *brip1 brip2*. A total of 827 peaks (dark blue dots) showed the same level of BRM occupancy in WT and *brip1 brip2*. FDR values are multiple test-corrected Wilcoxon test P values, two biological replicates per ChIP. **c**, Plot representation of the mean density of BRM occupancy at all BRM-occupied sites in *brip1 brip2* compared with WT. The average BRM binding signal within 3-kb genomic regions flanking BRM peak summits is shown. **d**, IGV views of BRM occupancy at selected loci in the WT and *brip1 brip2* background. The scale is identical for the different tracks, and gene structures are shown below each panel. The genes' ID and the 'START' and 'END' positions of the chromosome are shown below. The y-axis scales represent shifted merged MACS2 tag counts for every 10-bp window. **e**, ChIP-qPCR validation of BRM occupancy at shared targets using ChIP DNA samples independent from those used for ChIP-seq. Data are shown as the percentage of input. WT plants were used as the negative control sample, and the TA3 locus was used as the negative control locus. Error bars are presented as mean values \pm s.d. from three biological replicates. * $P < 0.05$, ** $P < 0.01$; NS, not significant (unpaired, two-tailed Student's t -test).

fewer peptides corresponding to various plant SWI/SNF subunits (Fig. 5e,f and Supplementary Table 4). In contrast, the total numbers of unique peptides, and peptides corresponding to the five most abundant proteins identified in input samples of *brip1 brip2* seedlings, were similar to those of WT (Extended Data Fig. 8a–c and Supplementary Table 4). Moreover, the total number of peptides in FLAG or GFP IP samples of the *brip1 brip2* mutant background was also similar to that of WT (Extended Data Fig. 8a and Supplementary Table 4), suggesting that the observed decreases in

protein levels were specific to SWI/SNF subunits. To further assess whether BRIP1/2 are required for the assembly of the SWI/SNF complexes, we introduced the SWI3C-FLAG transgene into the BRM-GFP line and used it for co-IP assay. Loss of BRIP1/2 resulted in substantially reduced protein levels for BRM-GFP and SWI3C-FLAG and reduced BRM subunit incorporation into the complexes, as shown by immunoprecipitation of SWI3C-FLAG (Fig. 5g). Together, these data suggest that BRIP1 and BRIP2 are required for the maintenance of SWI/SNF complexes, and that the reduction in

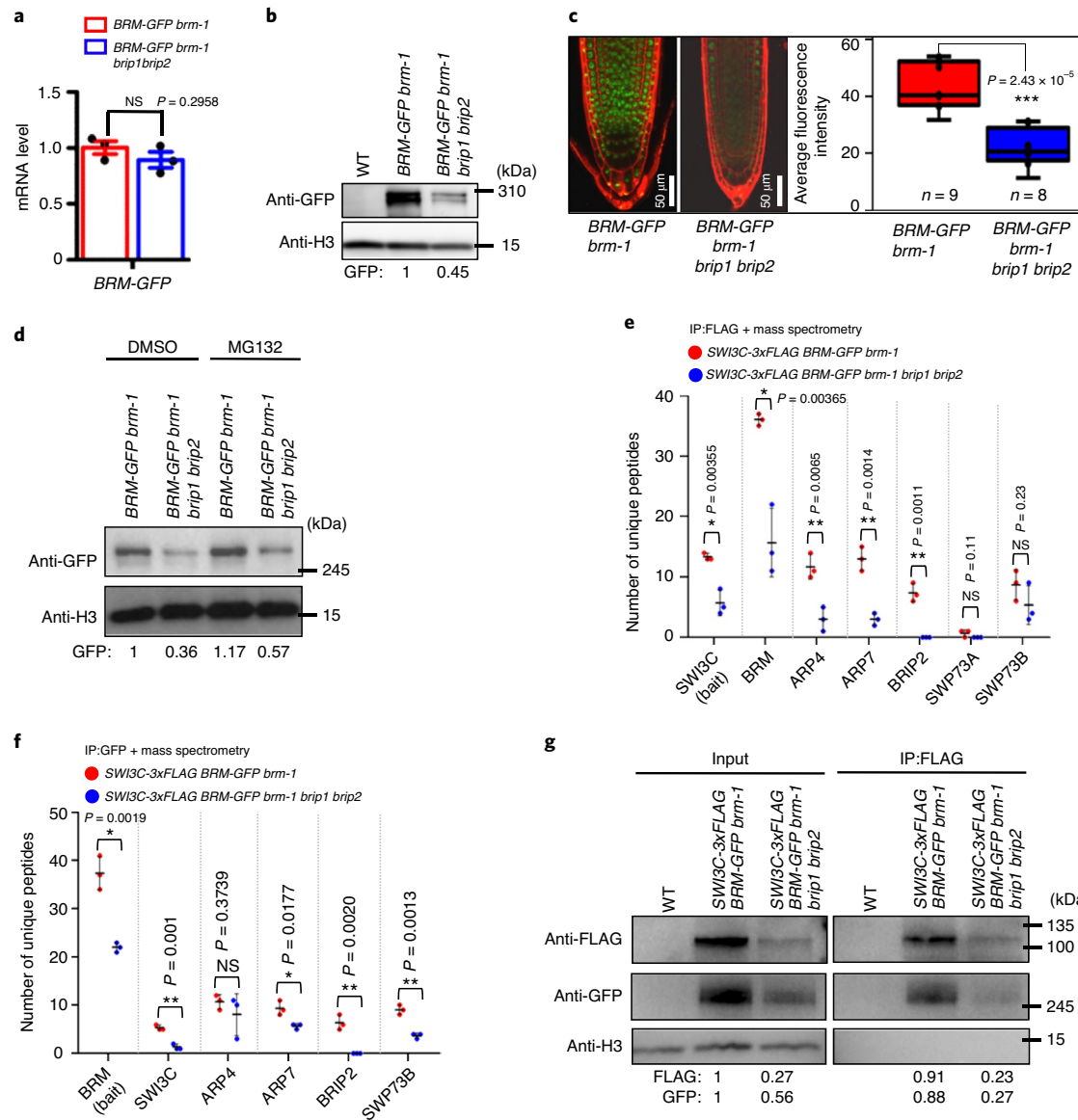


Fig. 5 | BRIP1 and BRIP2 are essential for the integrity of BRM complexes. **a**, The mRNA levels of BRM-GFP were determined by RT-PCR in a WT and *brip1 brip2* background. GAPDH was amplified as an internal control. Error bars are presented as mean values \pm s.d. from three biological replicates. **b**, Immunoblot analysis showing the relative protein levels of BRM-GFP in a WT and *brip1 brip2* background. The numbers at the bottom represent amounts normalized to the loading control, histone H3. WT is used as a GFP-free control. **c**, Left, confocal images of root tips showing nuclear localization of the BRM-GFP fusion protein in a WT and a *brip1 brip2* background, respectively. The red fluorescent signal is derived from propidium iodide staining. Right, box plot showing the average fluorescence intensity of BRM-GFP in WT and *brip1 brip2* mutants. *n*, number of roots used. The boxes indicate the first and third quartiles, and the whiskers indicate the minimum and maximum values. The lines in the boxes indicate median values. Significant differences were determined by unpaired, two-tailed Student's *t*-test, *** $P < 0.01$. **d**, Immunoblot analysis showing that MG132 treatment partially prevents BRM degradation. DMSO was used as a control. The numbers at the bottom represent amounts normalized to the loading control, histone H3. **e,f**, Mass spectrometry analysis showing a decreased number of peptides corresponding to SWI/SNF complex subunits recovered by immunoprecipitation of SWI3C-FLAG (**e**) or BRM-GFP (**f**) in *brip1 brip2* mutants. Error bars are presented as mean values \pm s.d. from three biological replicates, * $P < 0.05$, ** $P < 0.01$ (unpaired, two-tailed Student's *t*-test). **g**, Immunoblot showing the levels of SWI3C-3xFLAG and BRM-GFP from co-IP experiments with anti-FLAG antibody in the genetic backgrounds indicated above lanes. For each plot the antibody used is indicated on the left, and the sizes of the protein markers are indicated on the right. The numbers at the bottom represent amounts normalized to the loading control, histone H3.

BRM occupancy at target genes in the *brip1 brip2* mutants is probably due to reduced BRM protein levels.

The GLTSCR domain is essential for the function of BRIP2. To investigate the biological significance of the GLTSCR domain of BRIP proteins, we stably expressed a truncated version of BRIP2

lacking the GLTSCR domain under the control of its native promoter in *brip1 brip2* (hereafter referred to as BRIP2ΔGLTSCR) (Fig. 6a). The protein level of BRIP2ΔGLTSCR was much lower than that of BRIP2 (Fig. 6b,c), albeit with a moderate decrease in transcription level (Extended Data Fig. 9a). BRIP2ΔGLTSCR failed to rescue the downward-curled leaf and short siliques phenotypes of

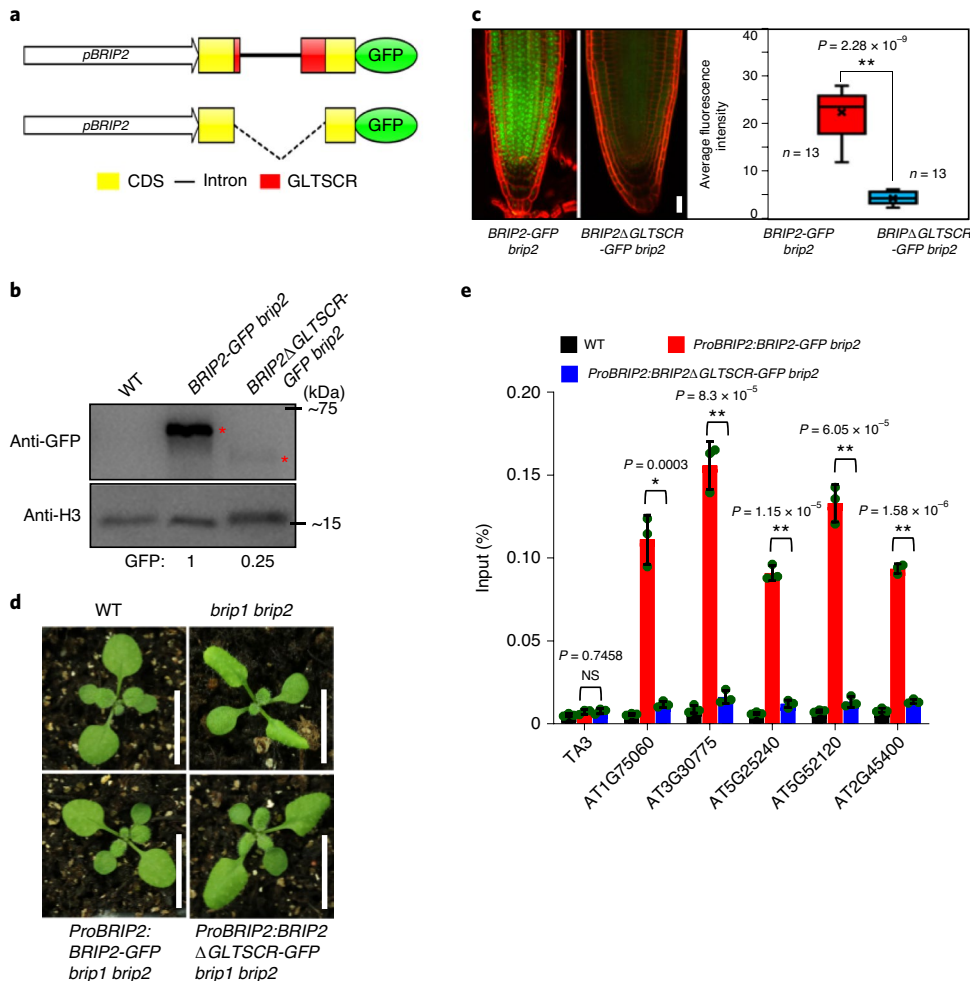


Fig. 6 | The GLTSCR domain is essential for the function of BRIP2. **a**, A schematic of proteins encoded by the transgene constructs. The conserved domains (GLTSCR) of BRIP2 are shown. **b**, Immunoblot analyses showing the relative protein levels of BRIP2-GFP and BRIP2ΔGLTSCR-GFP (numbers at the top represent amounts normalized to the loading control, histone H3). Red stars indicated the positions of proteins. **c**, Left, confocal images of root tips showing nuclear localization of BRIP2-GFP and BRIP2ΔGLTSCR-GFP. The red fluorescent signal is derived from propidium iodide staining. Scale bar, 50 μm. Right, box plots showing the average fluorescence intensity of BRIP2-GFP and BRIP2ΔGLTSCR-GFP. The numbers below indicate the number of root tips that were used. The boxes indicate the first and third quartiles, and the whiskers indicate the minimum and maximum values. The lines in the boxes indicate the median values and 'x' in the boxes indicates mean values. Significant differences were determined by unpaired, two-tailed Student's *t*-test, ** $P < 0.01$. **d**, Morphological phenotypes of WT, *brip1 bripl2*, *ProBRIP2:BRIP2-GFP bripl2* and *ProBRIP2:BRIP2ΔGLTSCR-GFP bripl2*. Photographs of 14-day-old plants are shown. Scale bars, 1 cm. **e**, ChIP-qPCR showing genomic occupancy by WT and GLTSCR-deleted BRIP2-GFP fusion proteins. WT was used as the negative control, and the TA3 locus was used as the negative control locus. Error bars are presented as mean values \pm s.d. from three biological replicates, * $P < 0.05$, ** $P < 0.01$ (unpaired, two-tailed Student's *t*-test).

brip1 bripl2 double mutants (Fig. 6d and Extended Data Fig. 9b,c), indicating that the GLTSCR domain is critical for the biological function of BRIP2. Furthermore, ChIP-qPCR analysis showed that BRIP2ΔGLTSCR was unable to occupy the genomic sites bound by the corresponding WT BRIP2, demonstrating that the GLTSCR domain is essential for the association of BRIP2 with chromatin (Fig. 6e).

Discussion

SWI/SNF complexes play critical roles in a wide range of developmental processes in plants; however, the subunit composition of plant SWI/SNF complexes is not yet fully elucidated, presenting a significant barrier to our understanding of the functions and effects of mutations on SWI/SNF complexes in plants. Here, we have identified two new core subunits of BRM-containing SWI/SNF complexes in plants and investigated the role of these subunits in the

complexes. Genetic, biochemical and genomic data demonstrated that BRIP1/2 are core components of plant SWI/SNF complexes that function to maintain the protein levels of the members of the BRM-containing SWI/SNF complexes, enabling them to associate with chromatin.

The GLTSCR domain-containing proteins are not found in yeast but are present in plants and animals^{9,10,36–38}. During the preparation of this manuscript, it was shown that mammalian SWI/SNF complexes could be divided into three distinct subcomplexes: BAF (cBAF), PBAF and a newly characterized non-canonical complex (GBAF, or ncBAF)³⁹. All three subcomplexes are composed of a subcomplex-specific core module and an ATPase module. Interestingly, GLTSCR1 and GLTSCR1L, the human homologues of *Arabidopsis* BRIP1/2, are present only in the GBAF subcomplex^{39–41}. As a result, GLTSCR1/1L co-localize a small portion (~15%) of sites occupied by the SMARCA4 (BRG1) ATPase subunit^{40,41}.

Furthermore, GLTSCR1/1L are not required for assembly of the ATPase module in humans³⁹. In contrast to their mammalian counterparts, BRIP1/2 extensively co-localize with the BRM ATPase subunit genome-wide, and plants lacking BRIP1/2 resemble *brm* mutants and show impairment in SWI/SNF occupancy at almost all BRM target genes. Moreover, BRIP1/2 are essential for maintaining the protein levels of the BRM ATPase and other core subunits. Our work suggests that plants and animals keep conserved subunits in their SWI/SNF complexes but have evolved distinct mechanisms to fulfil the subunit function within the complexes. This function of BRIP1/2 in *Arabidopsis* may be conserved in other plants: there are many homologous proteins of BRIP1/2 in diverse plant species, including angiosperms and bryophytes (*Physcomitrella patens*) (Extended Data Fig. 10).

In both *brip1* and *brip2* single mutants, more genes were down-regulated than upregulated (Extended Data Fig. 4a). Integrative analysis of genes displaying altered expression in *brip1* or *brip2* single mutants with genes occupied by BRIP1 or BRIP2, respectively, showed that there were probably more genes directly induced by BRIP1 or BRIP2 than those directly repressed (Supplementary Fig. 4a,b). This implies that BRIP1/2 tend to activate gene expression, though they can also repress transcription of certain genes. This is in line with published reports showing that BRM-containing SWI/SNF complexes can work as both activators and repressors of gene expression in plants^{15,42,43}. Interestingly, 77 genes were misregulated in *brip2* and also directly occupied by BRIP2 (Supplementary Fig. 4b). However, the overlapping between genes misexpressed in *brip1* and those directly occupied by BRIP1 was less significant (Supplementary Fig. 4a). This difference between the two implies that BRIP2 may be more important than BRIP1 in regulation of development. Consistent with this notion, *brip2* single mutants showed moderate early flowering while *brip1* mutants did not show visible phenotypes under our growth conditions (Extended Data Fig. 3c). These observations also suggest that, while BRIP1 and BRIP2 localize to a large number of genes across the genome, only a few of these target genes are differentially expressed in single mutants, which is in agreement with previous reports showing that the vast majority of genes occupied by SWI/SNF complexes do not show altered expression in SWI/SNF mutants in either plants or animals^{42,44}. It could also be due partially to the redundancy between BRIP1 and BRIP2 on gene expression regulation. Finally, our data show that BRIP1/2 accumulate at many key developmental genes (Extended Data Fig. 6c), the misregulation of which may be responsible for many of the phenotypes observed in *brip1 brip2* mutants. For example, growth-regulating factor 5 (GRF5) is a transcription factor that plays a role in stimulating *Arabidopsis* leaf development. The *grf5* single mutants exhibit smaller and narrow leaves, which are similar to *brip1 brip2* leaves⁴⁵. We found that the GRF5 gene was occupied by BRIP1/2 (Supplementary Table 3), and its transcription showed a marked reduction in *brip1 brip2* mutants compared with WT seedlings (Supplementary Table 2), providing a possible explanation for the leaf phenotype of *brip1 brip2* seedlings.

Our results show that the occupancy of BRM to target genes in *brip1 brip2* double mutants was substantially reduced compared to that in WT (Fig. 4). BRM protein levels (Fig. 5b,c) and the abundance of the SWI/SNF assemblies in *brip1 brip2* double mutants were also decreased (Fig. 5e–g). Thus, the reduction of BRM occupancy in *brip1 brip2* mutants is probably due to reduced BRM protein levels. It is still unknown how BRIP1/2 deletion causes reduction of BRM protein levels in the nucleus. The transcription level of *BRM* in *brip1 brip2* mutants was not different from that in WT, suggesting that the regulation of BRM protein levels by BRIP1/2 is not at the transcription level. It was recently shown that ubiquitination by 26S proteasome⁴⁶ and SUMOylation by AtMMS21 (ref. ³³) have a negative and positive effect, respectively, on the stability of BRM proteins. Testing whether BRIP1/2 mediate the abundance of SWI/SNF complexes by

affecting ubiquitination and/or SUMOylation of BRM would be a useful future direction.

Interestingly, we found that the enrichment signals of BRIP1 or BRIP2 at target genes were substantially decreased in the *brm-1* mutant compared to those in WT (Extended Data Fig. 7), suggesting that the BRM ATPase subunit may modulate the occupancy of BRIP1/2 and/or other subunits on chromatin in *Arabidopsis*. In humans, it was recently reported that the absence of ATPase subunits of SWI/SNF complexes led to decreased protein levels of the GLTSCR1 subunit³⁹. Furthermore, in the absence of ATPase subunits, human SWI/SNF complexes were reduced to a residual assembly with a low affinity to chromatin⁴⁷. It is possible that a similar mechanism may be present in plants, and warrants further studies.

Finally we show that the GLTSCR domain is essential for the biological function of BRIP1/2, because the reintroduction of GLTSCR-deficient BRIP2 failed to restore the phenotypes of *brip1 brip2* (Fig. 6d). Absence of the GLTSCR domain led to a reduction in BRIP2 protein levels (Fig. 6b). Moreover, the GLTSCR domain is specifically required and sufficient for interaction with BRM (Fig. 1e,f). Previous studies in mammals also showed that the GLTSCR domain is required for its interaction with GBAF complexes and serves as a GBAF-specific binding region^{36,41}. We speculate that the GLTSCR domain may play a role in organization of BRIP1/2-BRM complexes in plants and so, without the GLTSCR domain, BRIP1/2 may be disassociated from SWI/SNF complexes and thus become more susceptible to degradation. Further research is required to test this hypothesis.

It is notable that, because loss of BRIP1/2 did not lead to phenotypes as strong as *brm* null mutants and complete degradation of BRM-containing SWI/SNF complexes, additional core subunits besides BRIP1/2 probably exist in plants and remain to be characterized. Future identification and characterization of additional subunits, combined with our work presented here, should further enhance our understanding of plant SWI/SNF complexes.

Methods

Plant materials and cultivation conditions. *Arabidopsis* seeds were stratified for 4 d at 4 °C in darkness. All plant materials used in this study were in the Columbia-0 (Col-0) ecotype and, unless otherwise specified, plants were grown under 22 °C long-day conditions (16/8 h light/dark). For RT-qPCR/RNA-seq and ChIP-qPCR/ChIP-seq assays, seeds were sterilized in 20% sodium hypochlorite, sown on 1/2 Murashige and Skoog (MS) medium and grown for 14 d. For phenotypic analysis, seeds were sown directly on the soil. For protoplast experiments, plants were grown under 22 °C short-day conditions (12/12 h light/dark).

Transfer DNA insertion lines, *brip1-1* (SALK_133464) and *brip2-1* (SALK_177513) were obtained from the *Arabidopsis* Biological Resource Center (ABRC). Mutants *brm-1* (SALK_030046) and *brm-3* (SALK_088462) and *pBRM:BRM-GFP brm-1* transgenic plants were previously described^{12,34,48}. Oligonucleotide primers used for genotyping are listed in Supplementary Table 5.

Generation of transgenic plants. The *BRIP1* genomic regions corresponding to full-length *BRIP1*, including a 1.7-kb promoter and the coding region without the stop codon, were amplified and subcloned into the *pDONR221* vector by BP reaction (Invitrogen). The inserts were then transferred into the *pMDC107* vector⁴⁹ by LR reaction (to generate *pBRIP1:BRIP1-GFP*). The constructs were introduced into *Agrobacterium tumefaciens* strain GV3101 and were then used to transform *brip1 brip2* double mutant plants using the floral dip method⁵⁰. *pBRIP1:BRIP1-GFP brip1* was isolated after crossing *pBRIP1:BRIP1-GFP brip1 brip2* with *brm-1*.

For *BRIP2* and *BRIP2ΔGLTSCR*, genomic regions corresponding to full-length *BRIP2*, including a 2.0-kb promoter and the coding region without the stop codon, were amplified. Other operations were performed in the same way as for *BRIP1*. *pBRM:BRM-GFP brm-1 brip1 brip2*, *pBRIP1:BRIP1-GFP brip1 brm-1* and *pBRIP2:BRIP2-GFP brip2 brm-1* were generated through crossing.

For *SWI3C-3xFLAG BRM-GFP*, genomic regions corresponding to full-length *SWI3C*, including a 2.0-kb promoter and the coding region without the stop codon, were amplified and subcloned into *pZPY122-FLAG*⁵¹ (after cutting with restriction enzymes *KpnI* and *PstI*) using a homologous recombination with the ClonExpress Entry One Step Cloning Kit (Vazyme, no. C114). The construct was introduced into *A. tumefaciens* strain GV3101, which was used to transform *pBRM:BRM-GFP brm-1* transgenic plants using the floral dip method. *SWI3C-3xFLAG BRM-GFP*

brip1 brip2 was then obtained by crossing *SWI3C-3xFLAG BRM-GFP* with *brip1 brip2*.

β-Glucuronidase (GUS) staining. The promoters of *BRIP1* and *BRIP2* were amplified from the genomic DNA of Col-0 plants and were introduced into *pMDC162* (ref. ⁴⁹). The constructs were transformed into Col-0 using the floral dip method. GUS staining was performed following a previously described method⁵² with minor modifications. Transgenic plants were placed into the GUS staining solution (0.5 mg ml⁻¹ X-Glu, 0.1 M sodium phosphate buffer, 0.5 mM K₃Fe(CN)₆, 0.5 mM K₄Fe(CN)₆, 0.1% Triton X-100, 10% methanol and 10 mM EDTA), vacuum infiltrated for 15 min and then incubated at 37 °C overnight. After removal of chlorophyll by washing with 70% ethanol, photographs were taken with a SteREO Lumar V12 stereomicroscope (Zeiss).

RNA isolation, RT-qPCR and RNA-seq analyses. Total RNA was extracted using the RNAPrep Pure Plant Kit (Polysaccharides & Polyphenolics-rich, Vazyme, catalogue no. DP441, lot no. S7717) according to the manufacturer's instructions. RT-qPCR measurements were performed using either SYBR Green Supermix in the LightCycler480 system (Roche) or StepOne Plus (Applied Biosystems). Results were repeated with three independent RNA samples (biological replicates). Quantification was analysed with the relative -ΔΔCt method⁵³, using *GAPDH* as the internal control. The primers used for RT-qPCR are listed in Supplementary Table 5.

For transcriptome analysis, RNAs from three biological replicates were sequenced separately at Novogene, using Illumina Hiseq X-Ten (sequencing method: Hiseq-PE150). Reads were mapped to the TAIR10 *Arabidopsis* genome using TopHat⁵⁴ (Galaxy v.2.1.1 in <https://usegalaxy.org/>) with default settings, except that a minimum intron length of 20 base pairs (bp) and a maximum intron length of 4,000 bp were required (paired end). Mapped reads were then assembled according to the TAIR10 version of genome annotation using cufflinks⁵⁵ (v.2.1.1) with default settings. For analysis of differential expression, the assembled transcripts from three independent biological replicates in Col and other mutants were included and compared using Cuffdiff⁵⁵ (v.2.1.1) with default settings. Genes with at least 1.5-fold change in expression (*P*<0.05) were considered differentially expressed. To explore the relationships in transcriptomic changes among different mutants, genes with differential expression in at least one of the seven mutants (*brip1*, *brip2*, *brm-3*, *brm-1*, *brip1 brip2*, *brip1 brip2 brm-3*, *brip1 brip2 brm-1*) were collected, resulting in 3,455 genes which were further clustered via hierarchical clustering⁵⁶ and principal component analysis (PCA)⁵⁷ (<https://biit.cs.ut.ee/clustvis/>). To calculate the significance of the overlap of two groups of genes drawn from the set of genes, the total number of genes in the *Arabidopsis* genome used was 34,218 (27,655 coding and 6,563 non-coding genes) according to EnsemblPlants (<http://plants.ensembl.org/index.html>).

ChIP and ChIP-seq analysis. ChIP experiments were performed as previously described^{1,58,59}. Briefly, around 2 g of 14-day-old seedlings (each biological replication) grown on 1/2 MS culture medium was fixed using 1% formaldehyde under vacuum for 15 min. Chromatin was extracted and sonicated into ~200–500-bp fragments using the Bioruptor sonicator with a 30/30-s on/off cycle (total on cycles, 27) at the high setting. Immunoprecipitation was performed using 2 μl of anti-GFP (Abcam, no. ab290) at 4 °C overnight. DNA was purified using a MinElute PCR Purification Kit (Qiagen, catalogue no. 28004). ChIP-qPCR was performed with three technical replicates, and results were calculated as the percentage of input DNA according to the Champion ChIP-qPCR user manual (SABioscience). ChIP experiments were performed at least three times. The sequences of primers used for ChIP-qPCR are listed in Supplementary Table 5.

For ChIP-seq, 10 g of seedlings was used. End repair, adaptor ligation and amplification were carried out according to the manufacturer's protocol. Libraries were constructed by the NEBNext Ultra II DNA Library Prep Kit for Illumina (no. E7645L), NEBNext Multiplex Oligos for Illumina (no. E7335L) and VAHTS DNA Clean Beads (no. N411-02, Vazyme). High-throughput sequencing was carried out using Illumina Novaseq (sequencing method: Hiseq-PE150).

For ChIP-seq analysis, the raw reads were mapped to the reference genome (*Arabidopsis thaliana* genome, TAIR10) with Bowtie for Illumina⁶⁰ (Galaxy v.1.1.2) for DNA sequencing (<https://usegalaxy.org/>) with the default setting, except that the paired end was required. Unmapped and duplicated reads were then removed using SAMTools⁶¹. Only perfectly and uniquely mapped reads were retained for further analysis. A summary of the number of reads for each sample is given in Supplementary Table 6. MACS2 (refs. ^{62,63}) (Galaxy v.2.1.1) was used for peak calling using the following parameters: 'gsize=119,667,750, bw=300, q=0.01, nomodel, extsize=200'. The alignments were first converted to Wiggle (WIG) files, and bigwig files were generated using bamCoverage with '-bs 10' and '-normalizeUsing RPKM (reads per kilobase per million)' in DeepTools⁶⁴, and then the data were imported into the integrative genomics viewer (IGV)^{65,66} for visualization. For further analysis, only peaks that were present in both replicates (irreproducible discovery rate ≥ 0.05) were considered. To assign peaks to proximal genes, the online tool ChIPseeker⁶⁷ was used. The distance between the peak summit and nearby TSS of a gene was calculated. A peak summit positioned within 2 kb upstream or 2 kb downstream of a TSS was assigned to the corresponding

gene. Venn diagrams were created using BioVenn⁶⁸ (<http://www.biovenn.nl/index.php>). Differential occupancy of BRM in a WT and *brip1 brip2* background was determined using DiffBind⁶⁹ (Galaxy v.2.10.0), with default settings.

GO analysis. GO analysis for enriched biological processes was performed using TAIR (<https://www.arabidopsis.org>) and Metascape⁷⁰ (<http://metascape.org>), with default settings.

BiFC assays. Full-length coding sequences were amplified and cloned into the *pDONR221* vector by BP reaction. The resulting entry vectors were confirmed by sequencing to ensure that no errors were introduced by PCR amplification. The inserts were then transferred into the modified *pEarleyGate 201-nYFP* or *pEarleyGate 202-cYFP* vector⁷¹ by LR reaction. The constructs were introduced into *A. tumefaciens* strain *GV3101* individually, and the resulting bacteria were used to infiltrate the lower epidermis of tobacco (*Nicotiana benthamiana*) leaves. After 36–48 h, fluorescence signals were visualized using a confocal microscope (LSM880 with Fast airy scan). An unrelated nuclear protein encoded by *AT3G60390* was used as a negative control⁷¹. Sequences for the primers used are listed in Supplementary Table 5.

Y2H analysis. The entry vectors containing full-length or truncated complementary DNA were transferred into *pGADT7* or *pGBT7* by LR reaction. The Matchmaker Gold Y2H system (Clontech) was used for Y2H assay. The constructs were co-transformed into the Y2H Gold yeast strain that was selected on medium lacking leucine (Leu) and tryptophan (Trp). Positive colonies were picked up and dropped on the selection medium lacking adenine (Ade), histidine (His), Leu and Trp for image recording.

Co-immunoprecipitation and mass spectrometry. Full-length coding sequences of *BRIP2* were amplified from Col-0 cDNA and introduced into the *pHB-HA* vector⁷². The *pEAQ-BRM-N-GFP* vector containing the N-terminal (amino acids 1–952) of *BRM* was provided by S. Yang. The truncated versions of *BRIP2* were amplified and subcloned into *pHB-HA*⁷³ (after digestion by restriction enzyme BamHI) by homologous recombination with the ClonExpress Entry One Step Cloning Kit (Vazyme, no. C114). An 'ATG' start codon and a nuclear localization signal sequence of SV40 large T antigen (5'-ATG CCCAAAAAGAAGAGGAAAGTG-3') were added before the sequences of each truncated *BRIP2*. All primers used for vector construction are listed in Supplementary Table 5.

Transient expression assay was performed following a method previously described⁷⁴. Briefly, the constructs were co-transformed into *Arabidopsis* mesophyll protoplasts. For co-IP, protoplasts were harvested 12 h after transformation and lysed in IP buffer (10 mM HEPES, 10 mM NaCl, 1 mM EDTA, 10% glycerol, 0.5% Triton X-100, 25× complete protease inhibitor cocktail (Roche)). The lysate was centrifuged at 13,000g at 4 °C for 10 min. The supernatant was incubated with anti-HA-agarose antibody (Sigma, catalogue no. A2095-1ML, lot no. 048M4893V) for 3 h at 4 °C with rotation on a shaker. Finally, the beads were washed with wash buffer (IP buffer with 0.1% Triton X-100) three times and diluted in 5× SDS loading buffer followed by immunoblotting.

For co-IP of stable transgenic plants, nuclei were isolated from 2 g of 14-day-old *Arabidopsis* seedlings, squeezed 50 times with a tight pestle and then lysed with 2 ml of IP buffer (100 mM Tris-HCl pH 7.5), 300 mM NaCl, 2 mM EDTA, 1% Triton X-100, 10% glycerol, 1 mM phenylmethyl sulfonyl fluoride (PMSF) and 25× Complete protease inhibitor cocktail (Roche) at 4 °C for 30 min. After centrifugation at 5,000g at 4 °C for 10 min, the supernatant was incubated with 20 μl of Anti-FLAG Magnetic beads (Sigma, catalogue no. M8823) at 4 °C for 3 h and washed with washing buffer⁷⁵ (50 mM Tris-HCl pH 8.0), 150 mM NaCl, 5 mM MgCl₂, 1 mM DTT, 5% glycerol, 1 mM PMSF and 25× Complete protease inhibitor cocktail (Roche) three times. Finally, proteins were diluted in 5× SDS loading buffer without boiling, followed by immunoblotting.

Co-IP of HA-tagged truncated *BRIP2* and GFP-tagged *BRM-N* was performed in tobacco, as described above. Briefly, the constructs were co-transformed into tobacco leaves. Samples were collected after 36 h for co-IP using Anti-HA-Agarose antibody (Sigma, catalogue no. A2095-1ML, lot no. 048M4893V).

For mass spectrometry, equal amounts (4 g per sample) of 14-day-old control and mutant seedlings were used for nuclear extraction. Anti-FLAG Magnetic beads (Sigma, catalogue no. M8823) or anti-GFP was used for immunoprecipitation (KT Health, catalogue no. KTSIM1301, 1:5,000). The samples (including both input and IP) were analysed on a Thermo Scientific Q Exactive HF mass spectrometer in data-dependent mode. Spectral data were searched against the TAIR10 database using Protein Prospector 2.0. Three biological replicates were included in the IP-MS analysis. The mass spectrometry proteomics data have been deposited in the ProteomeXchange Consortium via the PRIDE partner repository⁷⁶, with the dataset identifier [PXD018815](https://doi.org/10.6090/PXD018815).

Immunoblotting. Proteins were resolved on 4–12% protein gels (GenScript, SurePAGE, catalogue no. M00653) and detected by anti-GFP (Abcam, no. ab290, lot no. GR3196305-1, 1:10,000 dilution), anti-FLAG (Sigma, catalogue no. A8592, 1:10,000 dilution), anti-FLAG (Ab-mart, catalogue no. M20008L, lot no. 304585,

1:10,000 dilution), anti-HA antibody (Sigma, catalogue no. H6533, 1:5,000 dilution) and anti-H3 (Proteintech, cat no. 17168-1-AP, 1:10,000 dilution). The intensity of blotting signals was quantified using ImageJ software v1.50i.

MG132 treatment assay. Around 2 g of 14-day-old seedlings vertically grown on 1/2 MS was transferred to a new 9×9-cm² Petri dish containing 50 ml of 40 µM MG132 (Abcam, lot no. APN17146-2-1), then horizontally shaken at 60 r.p.m. and 22 °C for 9 h. The same volume of DMSO was used as a control. Samples were frozen with liquid nitrogen. Nuclear proteins were extracted according to the ChIP assay protocol, followed by immunoblotting assay.

Assessment of flowering time and siliques length. Wild-type and mutant plants were grown side by side in soil at 22 °C with a 16/8-h light/dark cycle. The number of rosette leaves of each plant was determined when the first flower opened. The length of siliques for each genotype was measured when they turned fully brown.

Phylogenetic analysis. The amino acid sequences of the conserved GLTSCR domain from different species were download from <http://smart.embl-heidelberg.de/> and used for phylogenetic analysis. First, multiple-sequence alignment of the domains was performed using MEGA6 (ref. ⁷) with default parameters. Second, the phylogenetic tree was constructed with MEGA6 using the neighbour-joining method (bootstrap method (NO. of Bootstrap Replications, 500), Poisson model). Finally, the phylogenetic tree was beautified using Interactive Tree Of Life (iTOL)⁸ (<https://itol.embl.de/>).

Statistics and reproducibility. All statistics performed in this manuscript are detailed above, and statistical test methods, sample sizes and P values are indicated in the corresponding figure legends. Two-tailed Student's t-tests were conducted using Excel. P values for the Venn diagram overlap analysis are based on hypergeometric tests (http://nemates.org/MA/progs/overlap_stats.html). The post hoc Tukey honestly significant difference (HSD) test was performed with https://www.statsatistics.com/OneWay_Anova_with_TukeyHSD/. The experiments in Figs. 1c,e–g, 5b,d,g and 6b and Extended Data Figs. 1b, 2c, 3b and 5b,c were repeated at least three times independently, with similar results.

Reporting Summary. Further information on research design is available in the Nature Research Reporting Summary linked to this article.

Data availability

The ChIP-seq and RNA-seq datasets have been deposited in the Gene Expression Omnibus (GEO) under accession no. [GSE142369](https://www.ncbi.nlm.nih.gov/geo/query/acc.cgi?acc=GSE142369). The mass spectrometry proteomics data have been deposited in the ProteomeXchange Consortium under the dataset identifier [PXD018815](https://proteomecentral.proteomexchange.org/cgi/GetDataset?ID=PXD018815). Source data are provided with this paper.

Received: 30 December 2019; Accepted: 29 June 2020;

Published online: 3 August 2020

References

- Hargreaves, D. C. & Crabtree, G. R. ATP-dependent chromatin remodeling: genetics, genomics and mechanisms. *Cell Res.* **21**, 396–420 (2011).
- Clapier, C. R. & Cairns, B. R. The biology of chromatin remodeling complexes. *Annu. Rev. Biochem.* **78**, 273–304 (2009).
- Clapier, C. R., Iwasa, J., Cairns, B. R. & Peterson, C. L. Mechanisms of action and regulation of ATP-dependent chromatin-remodeling complexes. *Nat. Rev. Mol. Cell Biol.* **18**, 407–422 (2017).
- Ryan, D. P. & Owen-Hughes, T. Snf2-family proteins: chromatin remodelers for any occasion. *Curr. Opin. Chem. Biol.* **15**, 649–656 (2011).
- Ho, L. & Crabtree, G. R. Chromatin remodelling during development. *Nature* **463**, 474–484 (2010).
- Sarnowska, E. et al. The role of SWI/SNF chromatin remodeling complexes in hormone crosstalk. *Trends Plant Sci.* **21**, 594–608 (2016).
- Han, S. K., Wu, M. F., Cui, S. & Wagner, D. Roles and activities of chromatin remodeling ATPases in plants. *Plant J.* **83**, 62–77 (2015).
- Jerzmanowski, A. SWI/SNF chromatin remodeling and linker histones in plants. *Biochim. Biophys. Acta* **1769**, 330–345 (2007).
- Vercruyssen, L. et al. ANGUSTIFOLIA3 binds to SWI/SNF chromatin remodeling complexes to regulate transcription during *Arabidopsis* leaf development. *Plant Cell* **26**, 210–229 (2014).
- Nelissen, H. et al. Dynamic changes in ANGUSTIFOLIA3 complex composition reveal a growth regulatory mechanism in the maize Leaf. *Plant Cell* **27**, 1605–1619 (2015).
- Li, C. et al. Concerted genomic targeting of H3K27 demethylase REF6 and chromatin-remodeling ATPase BRM in *Arabidopsis*. *Nat. Genet.* **48**, 687–693 (2016).
- Li, C. et al. The *Arabidopsis* SWI2/SNF2 chromatin remodeler BRAHMA regulates polycomb function during vegetative development and directly activates the flowering repressor gene SVP. *PLoS Genet.* **11**, e1004944 (2015).
- Yang, S. et al. The *Arabidopsis* SWI2/SNF2 chromatin remodeling ATPase BRAHMA targets directly to PINs and is required for root stem cell niche maintenance. *Plant Cell* **27**, 1670–1680 (2015).
- Reyes, J. C. The many faces of plant SWI/SNF complex. *Mol. Plant* **7**, 454–458 (2014).
- Han, S. K. et al. The SWI2/SNF2 chromatin remodeling ATPase BRAHMA represses abscisic acid responses in the absence of the stress stimulus in *Arabidopsis*. *Plant Cell* **24**, 4892–4906 (2012).
- Farrona, S., Hurtado, L., Bowman, J. L. & Reyes, J. C. The *Arabidopsis thaliana* SNF2 homolog AtBRM controls shoot development and flowering. *Development* **131**, 4965–4975 (2004).
- Tang, X. et al. The *Arabidopsis* BRAHMA chromatin-remodeling ATPase is involved in repression of seed maturation genes in leaves. *Plant Physiol.* **147**, 1143–1157 (2008).
- Wu, M. F. et al. SWI2/SNF2 chromatin remodeling ATPases overcome polycomb repression and control floral organ identity with the LEAFY and SEPALLATA3 transcription factors. *Proc. Natl Acad. Sci. USA* **109**, 3576–3581 (2012).
- Zhang, D., Li, Y., Zhang, X., Zha, P. & Lin, R. The SWI2/SNF2 chromatin-remodeling ATPase BRAHMA regulates chlorophyll biosynthesis in *Arabidopsis*. *Mol. Plant* **10**, 155–167 (2017).
- Vicente, J. et al. The Cys-Arg/N-End rule pathway is a general sensor of abiotic stress in flowering plants. *Curr. Biol.* **27**, 3183–3190 (2017).
- Xu, Y. et al. Regulation of vegetative phase change by SWI2/SNF2 chromatin remodeling ATPase BRAHMA. *Plant Physiol.* **172**, 2416–2428 (2016).
- Wu, M. F. et al. Auxin-regulated chromatin switch directs acquisition of flower primordium founder fate. *eLife* **4**, e09269 (2015).
- Efroni, I. et al. Regulation of leaf maturation by chromatin-mediated modulation of cytokinin responses. *Dev. Cell* **24**, 438–445 (2013).
- Zhao, M. et al. *Arabidopsis* BREVIPEDICELLUS interacts with the SWI2/SNF2 chromatin remodeling ATPase BRAHMA to regulate KNAT2 and KNAT6 expression in control of inflorescence architecture. *PLoS Genet.* **11**, e1005125 (2015).
- Brzezinska, K. et al. *Arabidopsis* FORGETTER1 mediates stress-induced chromatin memory through nucleosome remodeling. *eLife* **5**, e17061 (2016).
- Sarnowska, T. J. et al. SWI3 subunits of putative SWI/SNF chromatin-remodeling complexes play distinct roles during *Arabidopsis* development. *Plant Cell* **17**, 2454–2472 (2005).
- Saez, A., Rodrigues, A., Santiago, J., Rubio, S. & Rodriguez, P. L. HAB1-SWI3B interaction reveals a link between abscisic acid signaling and putative SWI/SNF chromatin-remodeling complexes in *Arabidopsis*. *Plant Cell* **20**, 2972–2988 (2008).
- Archacki, R. et al. Genetic analysis of functional redundancy of BRM ATPase and ATSWI3C subunits of *Arabidopsis* SWI/SNF chromatin remodelling complexes. *Planta* **229**, 1281–1292 (2009).
- Sacharowski, S. P. et al. SWP73 subunits of *Arabidopsis* SWI/SNF chromatin remodeling complexes play distinct roles in leaf and flower development. *Plant Cell* **27**, 1889–1906 (2015).
- Buszewicz, D. et al. HD2C histone deacetylase and a SWI/SNF chromatin remodelling complex interact and both are involved in mediating the heat stress response in *Arabidopsis*. *Plant Cell Environ.* **39**, 2108–2122 (2016).
- Jegu, T. et al. The *Arabidopsis* SWI/SNF protein BAF60 mediates seedling growth control by modulating DNA accessibility. *Genome Biol.* **18**, 114 (2017).
- Oh, E., Zhu, J. Y. & Wang, Z. Y. Interaction between BZR1 and PIF4 integrates brassinosteroid and environmental responses. *Nat. Cell Biol.* **14**, 802–809 (2012).
- Zhang, J. et al. A SUMO ligase AtMMS21 regulates the stability of the chromatin remodeler BRAHMA in root development. *Plant Physiol.* **173**, 1574–1582 (2017).
- Hurtado, L., Farrona, S. & Reyes, J. C. The putative SWI/SNF complex subunit BRAHMA activates flower homeotic genes in *Arabidopsis thaliana*. *Plant Mol. Biol.* **62**, 291–304 (2006).
- Perez-Perez, J. M., Candela, H. & Micol, J. L. Understanding synergy in genetic interactions. *Trends Genet.* **25**, 368–376 (2009).
- Alpsoy, A. & Dykhuizen, E. C. Gloma tumor suppressor candidate region gene 1 (GLTSCR1) and its paralog GLTSCR1-like form SWI/SNF chromatin remodeling subcomplexes. *J. Biol. Chem.* **293**, 3892–3903 (2018).
- Ho, L. et al. An embryonic stem cell chromatin remodeling complex, esBAF, is essential for embryonic stem cell self-renewal and pluripotency. *Proc. Natl Acad. Sci. USA* **106**, 5181–5186 (2009).
- Middeljans, E. et al. SS18 together with animal-specific factors defines human BAF-type SWI/SNF complexes. *PLoS ONE* **7**, e33834 (2012).
- Mashhalir, N. et al. Modular organization and assembly of SWI/SNF family chromatin remodeling complexes. *Cell* **175**, 1272–1288 (2018).
- Gatchalian, J. et al. A non-canonical BRD9-containing BAF chromatin remodeling complex regulates naive pluripotency in mouse embryonic stem cells. *Nat. Commun.* **9**, 5139 (2018).

41. Michel, B. C. et al. A non-canonical SWI/SNF complex is a synthetic lethal target in cancers driven by BAF complex perturbation. *Nat. Cell Biol.* **20**, 1410–1420 (2018).
42. Archacki, R. et al. *Arabidopsis* SWI/SNF chromatin remodeling complex binds both promoters and terminators to regulate gene expression. *Nucleic Acids Res.* **45**, 3116–3129 (2017).
43. Torres, E. S. & Deal, R. B. The histone variant H2A.Z and chromatin remodeler BRAHMA act coordinately and antagonistically to regulate transcription and nucleosome dynamics in *Arabidopsis*. *Plant J.* **99**, 144–162 (2019).
44. Ho, L. et al. esBAF facilitates pluripotency by conditioning the genome for LIF/STAT3 signalling and by regulating polycomb function. *Nat. Cell Biol.* **13**, 903–913 (2011).
45. Horiguchi, G., Kim, G. T. & Tsukaya, H. The transcription factor AtGRF5 and the transcription coactivator AN3 regulate cell proliferation in leaf primordia of *Arabidopsis thaliana*. *Plant J.* **43**, 68–78 (2005).
46. Sakamoto, T., Tsujimoto-Inui, Y. & Sotta, N. Proteasomal degradation of BRAHMA promotes boron tolerance in *Arabidopsis*. *Nat. Commun.* **9**, 5285 (2018).
47. Pan, J., McKenzie, Z. M., D'Avino, A. R., Mashtalir, N. & Lareau, C. A. The ATPase module of mammalian SWI/SNF family complexes mediates subcomplex identity and catalytic activity-independent genomic targeting. *Nat. Genet.* **51**, 618–626 (2019).
48. Farrona, S., Hurtado, L. & Reyes, J. C. A nucleosome interaction module is required for normal function of *Arabidopsis thaliana* BRAHMA. *J. Mol. Biol.* **373**, 240–250 (2007).
49. Curtis, M. D. & Grossniklaus, U. A gateway cloning vector set for high-throughput functional analysis of genes in planta. *Plant Physiol.* **133**, 462–469 (2003).
50. Clough, S. J. & Bent, A. F. Floral dip: a simplified method for *Agrobacterium*-mediated transformation of *Arabidopsis thaliana*. *Plant J.* **16**, 735–743 (1998).
51. Liu, X. et al. The NF-YC-RGL2 module integrates GA and ABA signalling to regulate seed germination in *Arabidopsis*. *Nat. Commun.* **7**, 12768 (2016).
52. Adachi, S., Nobusawa, T. & Umeda, M. Quantitative and cell type-specific transcriptional regulation of A-type cyclin-dependent kinase in *Arabidopsis thaliana*. *Dev. Biol.* **329**, 306–314 (2009).
53. Livak, K. J. & Schmittgen, T. D. Analysis of relative gene expression data using real-time quantitative PCR and the 2(T)(-Delta Delta C) method. *Methods* **25**, 402–408 (2001).
54. Kim, D. et al. TopHat2: accurate alignment of transcriptomes in the presence of insertions, deletions and gene fusions. *Genome Biol.* **14**, R36 (2013).
55. Trapnell, C. et al. Transcript assembly and quantification by RNA-Seq reveals unannotated transcripts and isoform switching during cell differentiation. *Nat. Biotechnol.* **28**, 511–515 (2010).
56. Saeed, A. I. et al. TM4: a free, open-source system for microarray data management and analysis. *Biotechniques* **34**, 374–378 (2003).
57. Metsalu, T. & Vilo, J. ClustVis: a web tool for visualizing clustering of multivariate data using principal component analysis and heatmap. *Nucleic Acids Res.* **43**, W566–W570 (2015).
58. Gendrel, A. V., Lippman, Z., Martienssen, R. & Colot, V. Profiling histone modification patterns in plants using genomic tiling microarrays. *Nat. Methods* **2**, 213–218 (2005).
59. Chen, C. et al. Cytosolic acetyl-CoA promotes histone acetylation predominantly at H3K27 in *Arabidopsis*. *Nat. Plants* **3**, 814–824 (2017).
60. Langmead, B., Trapnell, C., Pop, M. & Salzberg, S. L. Ultrafast and memory-efficient alignment of short DNA sequences to the human genome. *Genome Biol.* **10**, R25 (2009).
61. Li, H. et al. The Sequence Alignment/Map format and SAMtools. *Bioinformatics* **25**, 2078–2079 (2009).
62. Zhang, Y. et al. Model-based analysis of ChIP-Seq (MACS). *Genome Biol.* **9**, R137 (2008).
63. Feng, J., Liu, T., Qin, B., Zhang, Y. & Liu, X. S. Identifying ChIP-seq enrichment using MACS. *Nat. Protoc.* **7**, 1728–1740 (2012).
64. Ramirez, F. et al. deepTools2: a next generation web server for deep-sequencing data analysis. *Nucleic Acids Res.* **44**, W160–W165 (2016).
65. Robinson, J. T. et al. Integrative genomics viewer. *Nat. Biotechnol.* **29**, 24–26 (2011).
66. Thorvaldsdottir, H., Robinson, J. T. & Mesirov, J. P. Integrative Genomics Viewer (IGV): high-performance genomics data visualization and exploration. *Brief. Bioinform.* **14**, 178–192 (2013).
67. Yu, G., Wang, L. G. & He, Q. Y. ChIPseeker: an R/Bioconductor package for ChIP peak annotation, comparison and visualization. *Bioinformatics* **31**, 2382–2383 (2015).
68. Hulsen, T., de Vlieg, J. & Alkema, W. BioVenn—a web application for the comparison and visualization of biological lists using area-proportional Venn diagrams. *BMC Genomics* **9**, 488 (2008).
69. Ross-Innes, C. S. et al. Differential oestrogen receptor binding is associated with clinical outcome in breast cancer. *Nature* **481**, 389–393 (2012).
70. Zhou, Y. Y. et al. Metascape provides a biologist-oriented resource for the analysis of systems-level datasets. *Nat. Commun.* **10**, 1523 (2019).
71. Lu, Q. et al. *Arabidopsis* homolog of the yeast TREX-2 mRNA export complex: components and anchoring nucleoporin. *Plant J.* **61**, 259–270 (2010).
72. Li, J. F., Zhang, D. D. & Sheen, J. Epitope-tagged protein-based artificial miRNA screens for optimized gene silencing in plants. *Nat. Protoc.* **9**, 939–949 (2014).
73. Liu, Y. C. et al. LjCOCH interplays with LjAPP1 to maintain the nodule development in *Lotus japonicus*. *Plant Growth Regul.* **85**, 267–279 (2018).
74. Yoo, S. D., Cho, Y. H. & Sheen, J. *Arabidopsis* mesophyll protoplasts: a versatile cell system for transient gene expression analysis. *Nat. Protoc.* **2**, 1565–1572 (2007).
75. Yang, Z. L. et al. EBS is a bivalent histone reader that regulates floral phase transition in *Arabidopsis*. *Nat. Genet.* **50**, 1247–1253 (2018).
76. Perez-Riverol, Y. et al. The PRIDE database and related tools and resources in 2019: improving support for quantification data. *Nucleic Acids Res.* **47**, D442–D450 (2019).
77. Tamura, K., Stecher, G., Peterson, D., Filipski, A. & Kumar, S. MEGA6: molecular evolutionary genetics analysis version 6.0. *Mol. Biol. Evol.* **30**, 2725–2729 (2013).
78. Letunic, I. & Bork, P. Interactive Tree Of Life (iTOL) v4: recent updates and new developments. *Nucleic Acids Res.* **47**, W256–W259 (2019).
79. Heger, A., Webber, C., Goodson, M., Ponting, C. P. & Lunter, G. GAT: a simulation framework for testing the association of genomic intervals. *Bioinformatics* **29**, 2046–2048 (2013).

Acknowledgements

We thank the ABRC for seeds of tDNA insertion lines, S. Yang and X. Hou (Chinese Academy of Sciences) for the pEAQ-BRM-N-GFP vector and pZPY122-FLAG vector, respectively, and J. Li (Sun Yat-sen University) for the pHBT-HA vector. This work was supported by the National Natural Science Foundation of China to C.L. (no. 31870289) and the Natural Science and Engineering Council of Canada to Y.C. (no. RGPIN/04625-2017).

Author contributions

Y.Y. and C.L. conceived the project. Y.Y. performed most of the experiments. Wenqun Fu constructed the GUS reporter lines. Y.Y., Z.L., L.Y. and C.L. conducted bioinformatics analysis. Y.Y., Z.L., X.S., Wei Fu, Y.L., L.Y., J.X., J.R., C.C., Y.C. and S.H. analysed data. Y.Y. and C.L. wrote the manuscript.

Competing interests

The authors declare no competing interests.

Additional information

Extended data is available for this paper at <https://doi.org/10.1038/s41477-020-0734-z>.

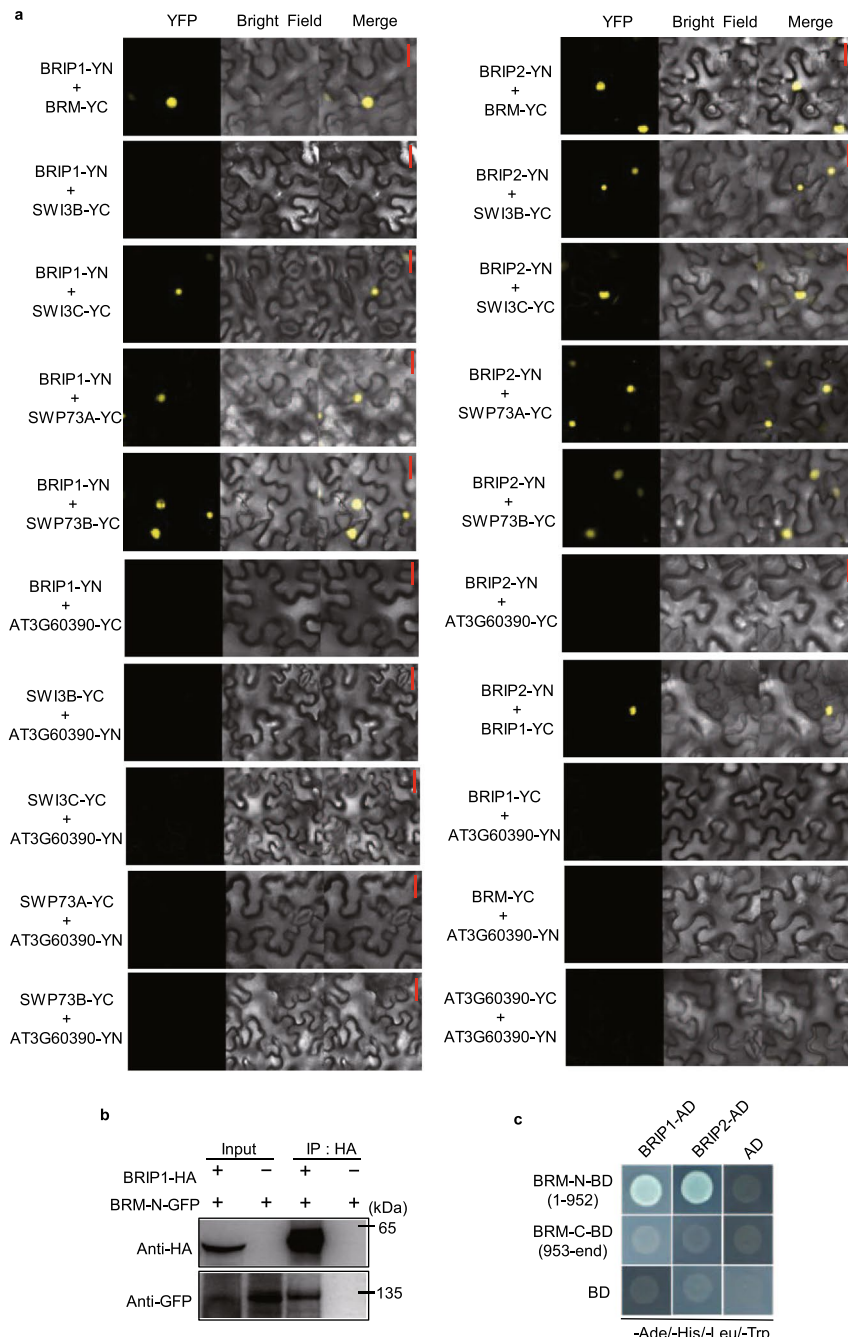
Supplementary information is available for this paper at <https://doi.org/10.1038/s41477-020-0734-z>.

Correspondence and requests for materials should be addressed to C.L.

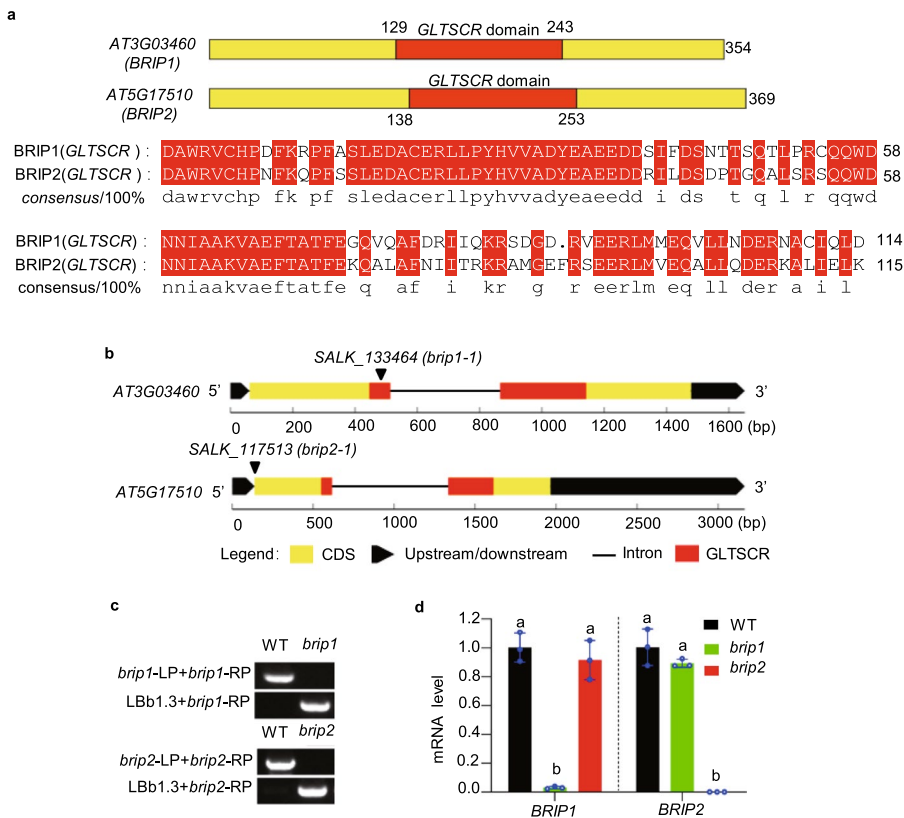
Reprints and permissions information is available at www.nature.com/reprints.

Publisher's note Springer Nature remains neutral with regard to jurisdictional claims in published maps and institutional affiliations.

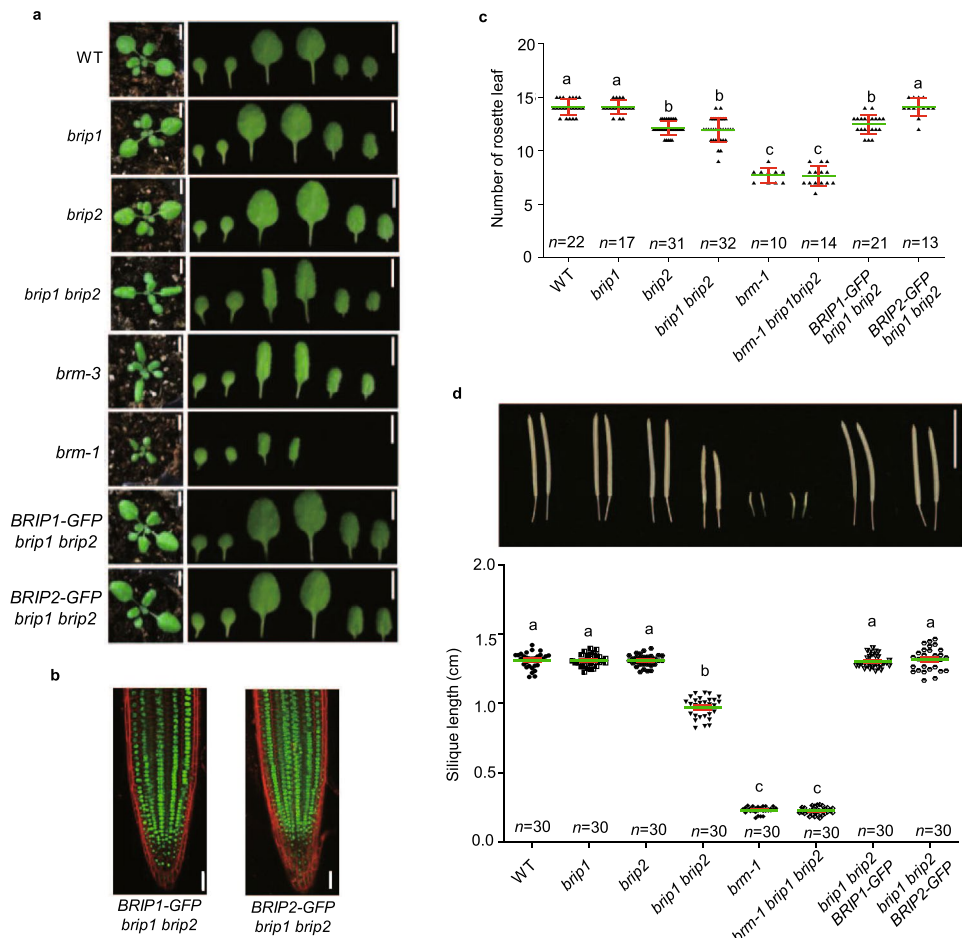
© The Author(s), under exclusive licence to Springer Nature Limited 2020



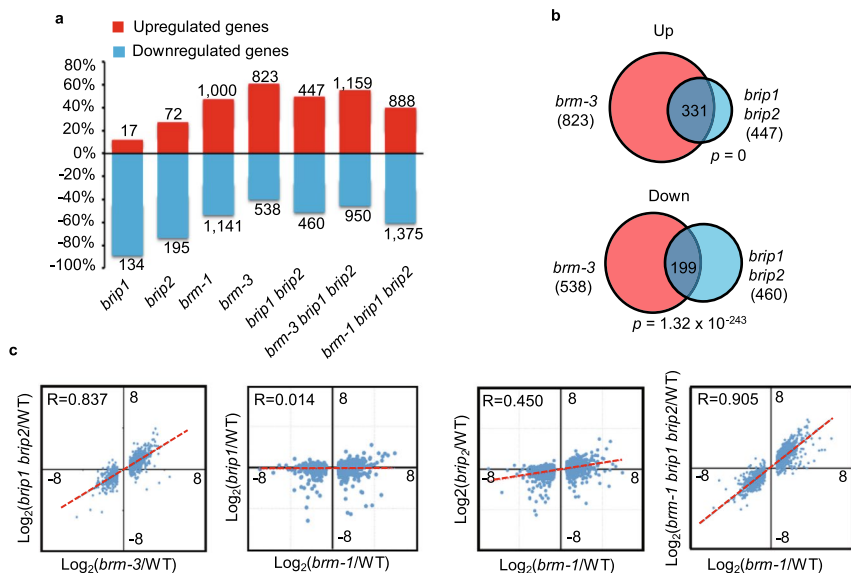
Extended Data Fig. 1 | Physical interaction among BRIP1, BRIP2 and SWI/SNF complex. **a**, Bimolecular Fluorescence Complementation assay (BiFC) showing that BRIP1 and BRIP2 interact with SWI/SNF complex core members. An unrelated nuclear protein encoded by AT3G60390 was used as a negative control. error bar = 20 μ m. **b**, Co-immunoprecipitation of BRIP1 with BRM-N (N-terminal of BRM, 1-952 amino acids). BRM-N-GFP was immunoprecipitated by an anti-HA-Agarose antibody from protoplasts co-transfected with BRM-N-GFP and BRIP1-HA. The antibodies used for immunoblot are indicated on the left, and the sizes of the protein markers are indicated on the right. **c**, Yeast-two hybrid assay to examine the region of BRM that interacts with BRIP1/2. Growth of transformed yeast is shown on permissive SD -Ade/-His/-Leu/-Trp medium.



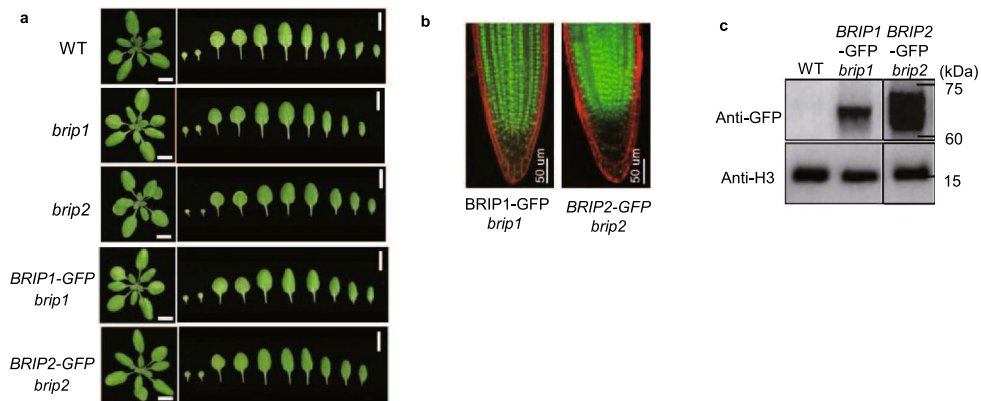
Extended Data Fig. 2 | Gene structures and Genetic materials. **a**, Schematic illustration of the conserved domain of BRIP1 and BRIP2. The numbers indicate the positions of amino acids. At the bottom, the alignment of the sequences of the GLTSCR domain of BRIP1/2 proteins. The amino acids same in both proteins are marked by red. **b**, Schematic illustration of the locations of the T-DNA insertion sites (dark arrow) of the two *brip* mutants. The GLTSCR domains are red marked. **c**, Genotyping of *brip1* and *brip2* by using the three primers method (LBb1.3+LP+RP). Wild-type (Col-0) was used as a control. **d**, The mRNA levels of *BRIP1* and *BRIP2* were determined by RT-PCR in *brip1*, *brip2* and Col-0. GAPDH was amplified as an internal control. Error bars represent s.d. of three biological replicates, as determined by the post hoc Tukey's HSD test.



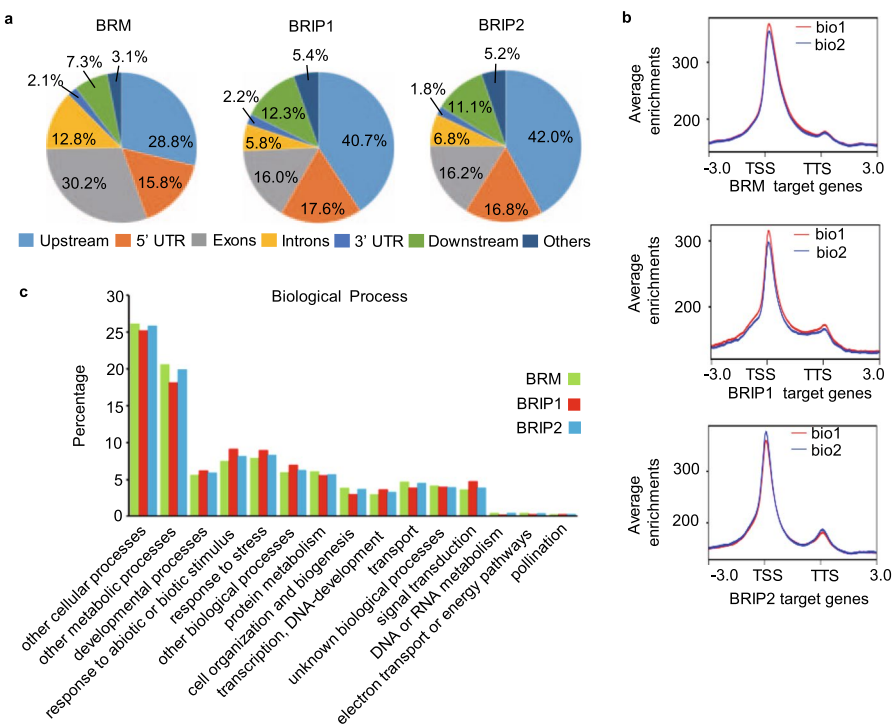
Extended Data Fig. 3 | Phenotype of *bripl*, *bripl2*, *bripl bripl2* and *brm* mutants. **a**, Leaf phenotype of 14-day-old seedlings. Scale bars, 5 mm. **b**, Confocal images of root tips showing nuclear localization of the BRIP1-GFP and BRIP2-GFP in *bripl bripl2* double mutant background. The red fluorescent signal is from propidium iodide staining. Scale bars, 50 µm. **c**, Number of rosette leaf of different plant materials at flowering. **d**, Siliques phenotypes of different materials. Scale bars, 1 cm. Lowercase letters indicate significant differences between genetic backgrounds, as determined by the *post hoc* Tukey's HSD test. The number of 'n=' indicates the number of plants that were used. Data are presented as mean values \pm SD.



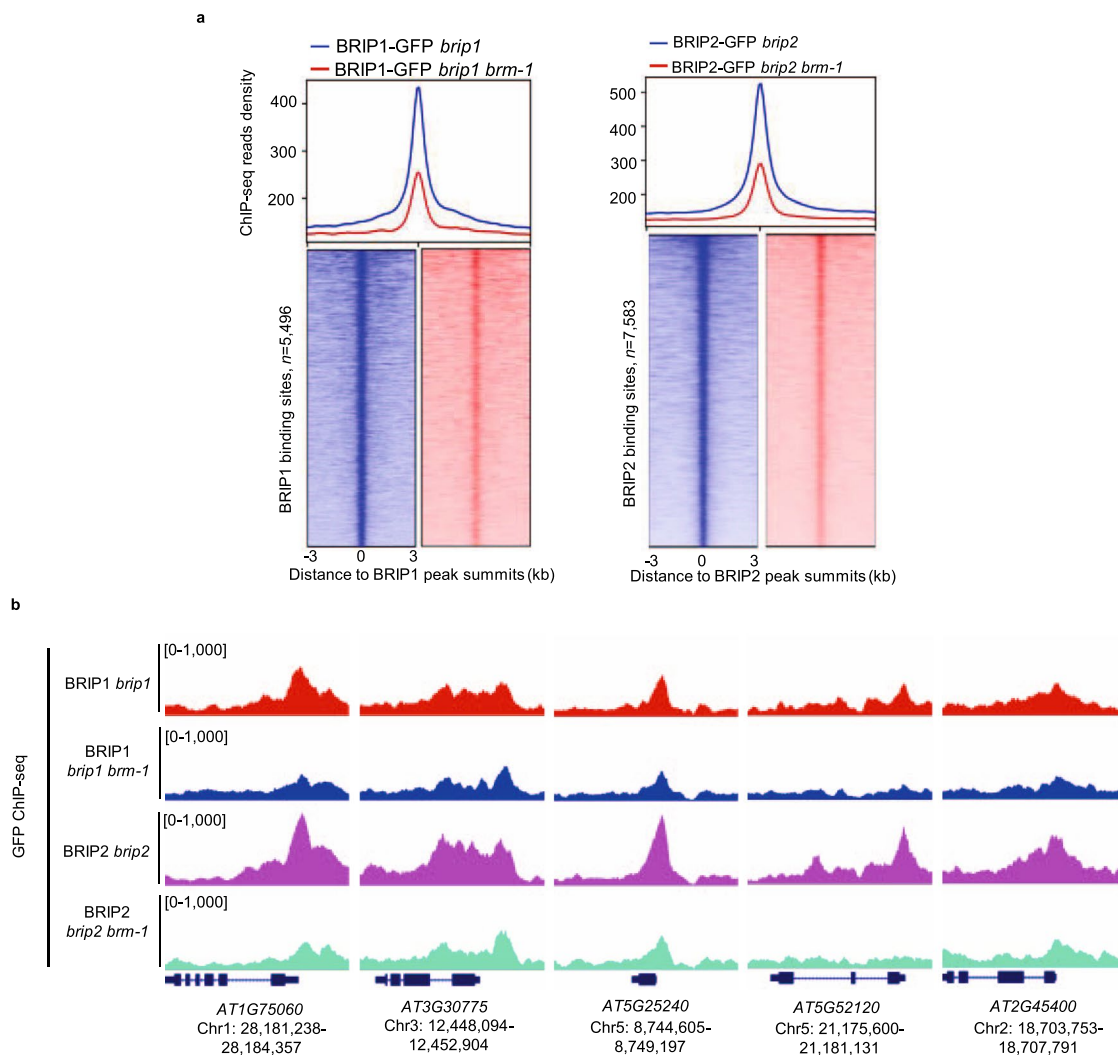
Extended Data Fig. 4 | *brrip1brrip2* mutants had similar transcriptome to *brm* mutants. **a**, Summary of up- and down-regulated genes in different mutants compared to WT. The number indicates the concrete number of up- and down-regulated genes and the Y-axis showing the percentage of up- and down-regulated genes of all mis-regulated genes. **b**, Venn diagrams showing statistically significant overlaps between genes up- or down-regulated in *brm-3* and those in *brrip1 brrip2*. $p = 0$, Hypergeometric test. **c**, Scatterplot of FPKM log₂ fold change over WT of indicated mutants (y-axis) vs. *brm-3* or *brm-1* (x-axis) at *brm-3* or *brm-1* differentially expressed genes. Red lines indicate the line of best fit, and adjusted R value is indicated. Dots are mean values from three biologically independent experiments.



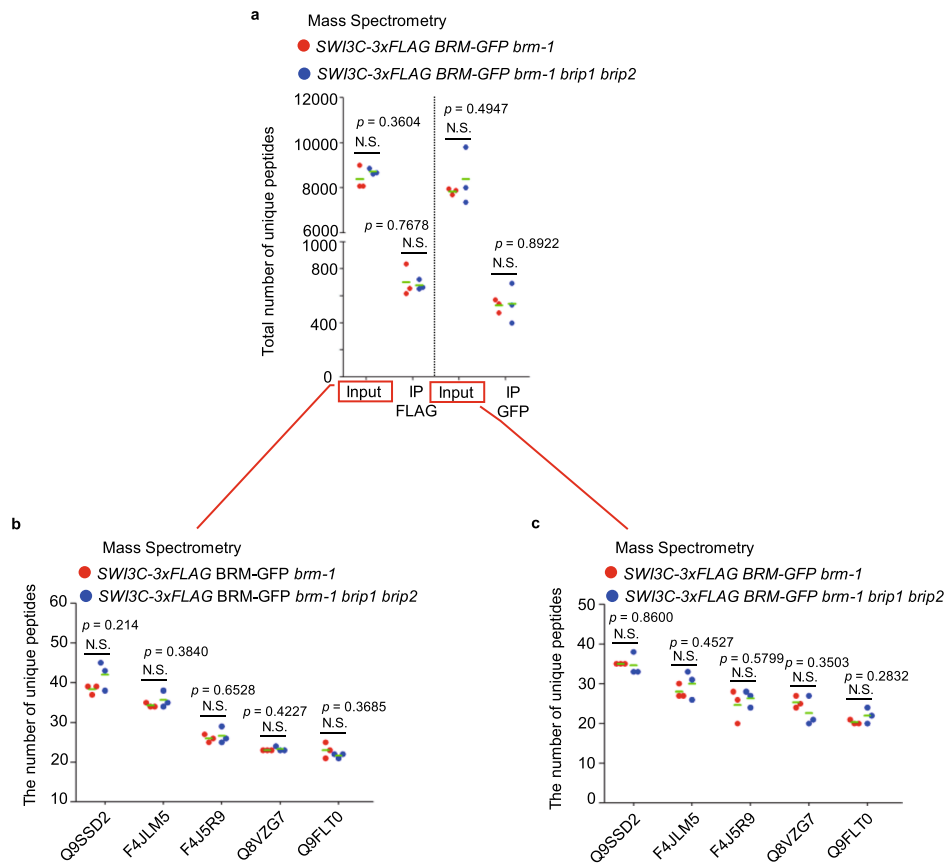
Extended Data Fig. 5 | Plants expressing GFP-tagged BRIP1 or BRIP2 in their respective single mutant background. **a**, Pictures showing 21-day-old plants. Scale bars, 1 cm. **b**, Confocal images of root tips showing nuclear localization of the BRIP1-GFP and BRIP2-GFP in their single mutant background. The red fluorescent signal is from propidium iodide staining. Scale bars, 50 μ m. **c**, Western blot analysis using an anti-GFP antibody shows the accumulation of BRIP1 and BRIP2. For each plot, the antibody used is indicated on the left, and the sizes of the protein markers are indicated on the right. H3 serves as a loading control.



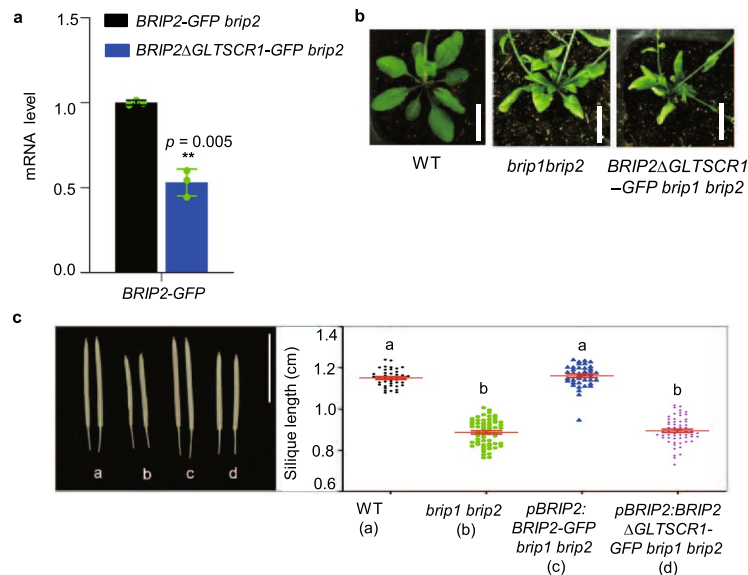
Extended Data Fig. 6 | BRIP1, BRIP2 and BRM show a similar binding pattern. **a**, Pie charts showing the distribution of BRM, BRIP1 and BRIP2 peaks at annotated genic and intergenic regions in the genome. **b**, The average enrichment of BRM, BRIP1 or BRIP2 at its target genes, respectively ($n=7,767, 5,035$ and $7,023$, respectively). Plotting regions were scaled to the same length as follows: 5' ends (-3.0 kb to transcription starting site (TSS)) and 3' ends (transcription stop site (TTS) to downstream 3.0 kb), and the gene body was scaled to 3 kb . Two biological replicates were included. **c**, GO analysis for biological processes associated with genes occupied by BRM, BRIP1 or BRIP2.



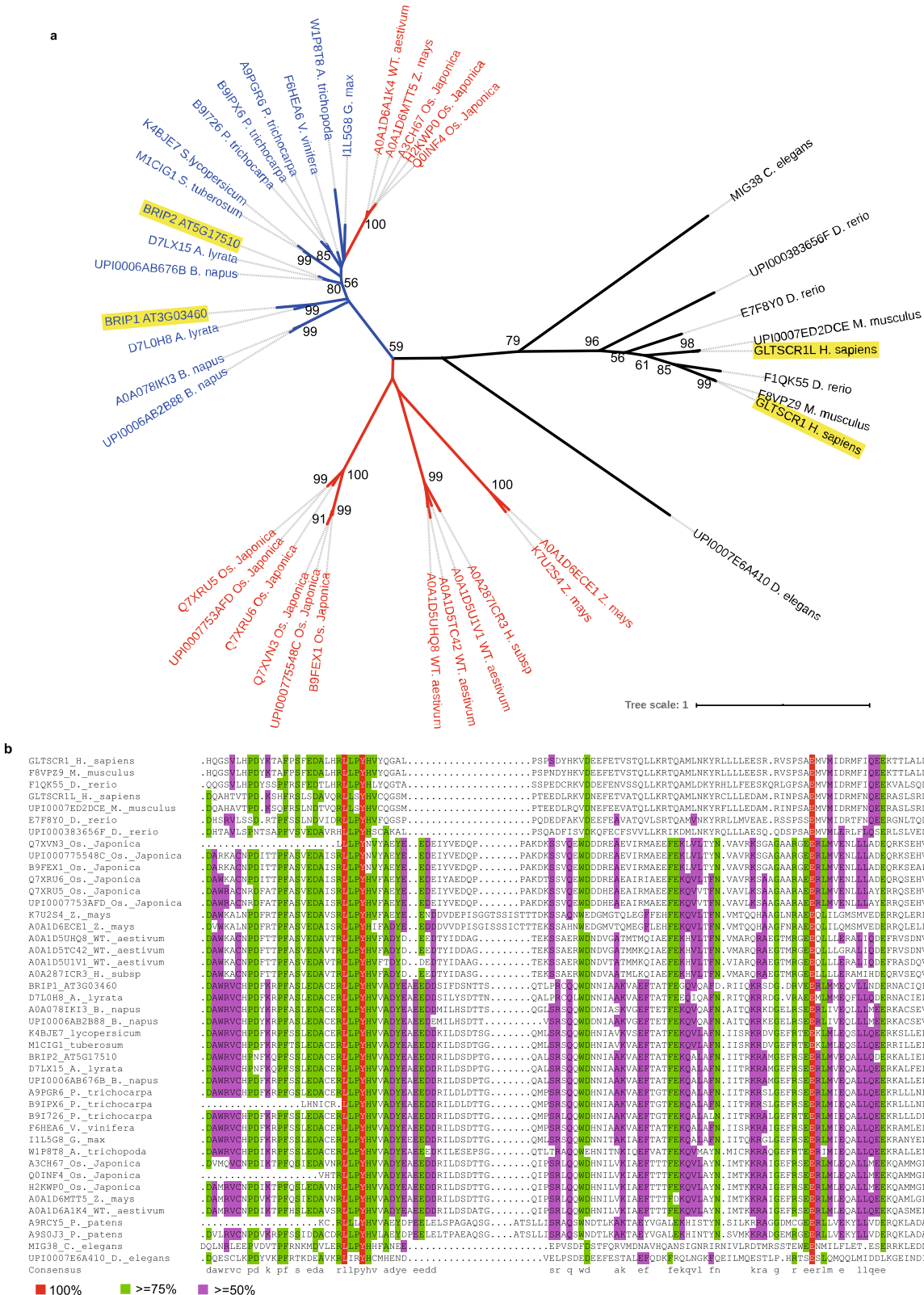
Extended Data Fig. 7 | Loss of BRM causes the genome-wide decrease of BRIP1/2 occupancy. **a**, On the top, Plot representation of the mean density of BRIP1 or BRIP2 occupancy at all BRIP1 or BRIP2 sites in *brm-1* compared with WT. The average BRIP1/2 binding signal within 3 kb genomic regions flanking the summit of BRIP1/2 peaks are shown. Bottom, Heat-map representation of the occupancy of BRIP1 or BRIP1 in WT and *brm-1*. **b**, IGV views of BRIP1/2 occupancy at selected loci in WT and *brm-1* background. The scale was identical for the different tracks, and gene structures are shown underneath each panel. The gene IDs and the 'START and END' positions on the chromosome are shown below. The y-axis scales represent shifted merged MACS2 tag counts for every 10-bp window.



Extended Data Fig. 8 | The number of unique peptides identified by Mass spectrometry analyses. **a**, Mass spectrometry results showing the total number of unique peptides in the input or IP samples of SWI3C-3xFLAG BRM-GFP *brm-1* and SWI3C-3xFLAG BRM-GFP *brm-1 bripl bripl2*. **b**, The number of unique peptides of five representative proteins (named by UniProt) in the input samples SWI3C-3xFLAG BRM-GFP *brm-1* before FLAG immunoprecipitation was similar to that in SWI3C-3xFLAG BRM-GFP *brm-1 bripl bripl2*. **c**, The number of unique peptides of five representative proteins (named by UniProt) in the input samples SWI3C-3xFLAG BRM-GFP *brm-1* before GFP immunoprecipitation was similar to that in SWI3C-3xFLAG BRM-GFP *brm-1 bripl bripl2*. Error bars are presented as mean values from three biological replicates, \pm SD. N.S., not significant (Unpaired, two-tailed Student's t-test).



Extended Data Fig. 9 | Loss of GLTSCR domain impairs the function of BRIP2. **a**, qRT-PCR analyses showing the mRNA level of *BRIP2ΔGLTSCR1-GFP* and full length *BRIP2-GFP*. The expression level of each gene was normalized to that of *GAPDH*. Error bars are presented as mean values from three biological replicates, $+/-$ SD. ** $p < 0.01$ (Unpaired, two-tailed Student's t-test). **b**, Morphological phenotypes of *pBRIP2:BRIP2-GFP bripl bripl* and *pBRIP2:BRIP2ΔGLTSCR1-GFP bripl bripl*. Photographs of 35-day-old plants are shown. Scale bar, 1 cm. **c**, Silique phenotypes of different materials. Scale bars, 1 cm. Lowercase letters indicate significant differences between genetic backgrounds, as determined by the post hoc Tukey's HSD test. The number of ' $n =$ ' indicates the number of plants that were used. Data are presented as mean values $+/-$ SD.



Extended Data Fig. 10 | Phylogenetic analysis of GLTSCR domain-containing proteins among different species. **a**, The phylogenetic tree was constructed using the amino-acid sequences of the GLTSCR domain from different species, including Amborella trichopoda, Physcomitrella patens, Arabidopsis thaliana, Arabidopsis lyrata, Brassica napus, Oryza sativa Japonica, Triticum aestivum, Hordeum vulgare subsp. Vulgare, Zea mays, Homo sapiens, Danio rerio, Drosophila melanogaster, Caenorhabditis elegans, Mus musculus. The scale length in the tree is indicated. **b**, The alignment of sequences of GLTSCR domain across different species. Conserved amino acids are marked in red (100%), green ($\geq 75\%$), and purple ($\geq 50\%$), respectively.

Reporting Summary

Nature Research wishes to improve the reproducibility of the work that we publish. This form provides structure for consistency and transparency in reporting. For further information on Nature Research policies, see [Authors & Referees](#) and the [Editorial Policy Checklist](#).

Statistics

For all statistical analyses, confirm that the following items are present in the figure legend, table legend, main text, or Methods section.

n/a Confirmed

- The exact sample size (n) for each experimental group/condition, given as a discrete number and unit of measurement
- A statement on whether measurements were taken from distinct samples or whether the same sample was measured repeatedly
- The statistical test(s) used AND whether they are one- or two-sided
Only common tests should be described solely by name; describe more complex techniques in the Methods section.
- A description of all covariates tested
- A description of any assumptions or corrections, such as tests of normality and adjustment for multiple comparisons
- A full description of the statistical parameters including central tendency (e.g. means) or other basic estimates (e.g. regression coefficient) AND variation (e.g. standard deviation) or associated estimates of uncertainty (e.g. confidence intervals)
- For null hypothesis testing, the test statistic (e.g. F , t , r) with confidence intervals, effect sizes, degrees of freedom and P value noted
Give P values as exact values whenever suitable.
- For Bayesian analysis, information on the choice of priors and Markov chain Monte Carlo settings
- For hierarchical and complex designs, identification of the appropriate level for tests and full reporting of outcomes
- Estimates of effect sizes (e.g. Cohen's d , Pearson's r), indicating how they were calculated

Our web collection on [statistics for biologists](#) contains articles on many of the points above.

Software and code

Policy information about [availability of computer code](#)

Data collection

Illumina Novaseq; Illumina Hiseq X-Ten; Thermo Scientific Q Exactive HF; LightCycler480 system (Roche) or StepOne Plus (Applied Biosystems); Leica LSM880

Data analysis

RNA-seq analysis: TopHat version 2.1.1, cufflinks version 2.1.1, Cuffdiff version 2.1.1
 ChIP-seq analysis: Bowtie for Illumina version 1.1.2, SAMTools version 3.3.0.0.0, MACS2 version 1.1.2, DeepTools version 2, Integrative Genomics Viewer (version 2.4.14), ChIPseeker Version 1.18.0+galaxy1, DiffBind version 2.10.0
 GO analysis: Metascape, <http://metascape.org>
 Phylogenetic analysis: MEGA6
 Confocal microscopy: LSM880 with Fast airy scan
 Western blot: Molecular Imager ChemiDoc XRХ+(BIO-RAD); Image lab 5.0
 IP-MS: Protein Prospector 2.0
 Others: ImageJ (1.50i), BioVenn (2007), Excel (2016), StepOne Software (v2.3)

For manuscripts utilizing custom algorithms or software that are central to the research but not yet described in published literature, software must be made available to editors/reviewers. We strongly encourage code deposition in a community repository (e.g. GitHub). See the Nature Research [guidelines for submitting code & software](#) for further information.

Data

Policy information about [availability of data](#)

All manuscripts must include a [data availability statement](#). This statement should provide the following information, where applicable:

- Accession codes, unique identifiers, or web links for publicly available datasets
- A list of figures that have associated raw data
- A description of any restrictions on data availability

Fig2, Fig3, Fig4, Extended Data Fig4, and Extended Data Fig6 have associated ChIP-seq and RNA-seq raw data, which have been deposited in the Gene Expression Omnibus (GEO) under accession GSE142369.

The mass spectrometry proteomics data in Fig5 and Extended Data Fig. 8 have been deposited to the ProteomeXchange Consortium via the PRIDE partner repository with the dataset identifier PXD018815.
 Ensemble, <http://plants.ensembl.org/index.html>;
 EMBL, <http://smart.embl-heidelberg.de/>

Field-specific reporting

Please select the one below that is the best fit for your research. If you are not sure, read the appropriate sections before making your selection.

Life sciences Behavioural & social sciences Ecological, evolutionary & environmental sciences

For a reference copy of the document with all sections, see nature.com/documents/nr-reporting-summary-flat.pdf

Life sciences study design

All studies must disclose on these points even when the disclosure is negative.

Sample size	For the assessment of flowering time and siliques length, wild-type and mutant plants were grown side by side on the soil at 22 °C with 16-h light/8-h dark cycles, at least 10 plants (ranging from 10 to 32 plants for different genotypes) were then used for the measurement. The number of plants for each genotype was provided in the manuscript. We determined the final sample sizes to be adequate based on the statistically significant differences in genotypes. For ChIP-seq and IP-MS, at least 500 14-day-old seedlings were collected for each sample. For RNA-seq, approximately 20 seedlings were used for RNA extraction. RNA-seq and IP-MS data contain at least three biological replicates from independent experiments.
Data exclusions	No data exclusion
Replication	Three biological replicates were used for ChIP-qPCR, RT-qPCR, RNA-seq, IP-MS. Two biological replicates were used for ChIP-seq. All attempts at replication were successful.
Randomization	wild-type and mutant plants were grown side by side on the soil at 22 °C with 16-h light/8-h dark cycles, the plants were then randomly collected for experiments.
Blinding	Experiments were not blinded. Data were always collected according to the genotype of plants.

Reporting for specific materials, systems and methods

We require information from authors about some types of materials, experimental systems and methods used in many studies. Here, indicate whether each material, system or method listed is relevant to your study. If you are not sure if a list item applies to your research, read the appropriate section before selecting a response.

Materials & experimental systems		Methods	
n/a	Involved in the study	n/a	Involved in the study
<input type="checkbox"/>	<input checked="" type="checkbox"/> Antibodies	<input type="checkbox"/>	<input checked="" type="checkbox"/> ChIP-seq
<input checked="" type="checkbox"/>	<input type="checkbox"/> Eukaryotic cell lines	<input checked="" type="checkbox"/>	<input type="checkbox"/> Flow cytometry
<input checked="" type="checkbox"/>	<input type="checkbox"/> Palaeontology	<input checked="" type="checkbox"/>	<input type="checkbox"/> MRI-based neuroimaging
<input checked="" type="checkbox"/>	<input type="checkbox"/> Animals and other organisms		
<input checked="" type="checkbox"/>	<input type="checkbox"/> Human research participants		
<input checked="" type="checkbox"/>	<input type="checkbox"/> Clinical data		

Antibodies

Antibodies used	anti-GFP (Abcam, Cat#ab290, Lot#GR3196305-1), Anti-FLAG Magnetic Beads (Sigma, Cat#M8823); anti-FLAG (Sigma, Cat# A8592); anti-FLAG (Ab-mart, Cat#M20008L, Lot#304585); Anti-HA-Agarose antibody (Sigma, Cat#A2095, Lot#048M4893V), Anti-HA antibody (Sigma, Cat#H6533), Anti-GFP (KT Health, Cat# KTS1301), and anti-H3 (Proteintech, Cat #:17168-1-AP)
Validation	<p>1. Anti-GFP antibody - ChIP Grade (ab290) is a highly versatile antibody that gives a stronger signal than other anti-GFP antibodies available. Suitable for: Flow Cyt, ELISA, ICC/IF, ChIP, IHC-FrFl, ChIP/Chip, IHC-Wholemount, Electron Microscopy, IHC-FoFr, ICC, IHC-P, IHC-Fr, IP, WB. The anti-GFP antibody was validated in Li et al., 2016 Nature Genetics.</p> <p>2. Anti-FLAG Magnetic Beads (Sigma, Cat#M8823) provide an easy, fast and convenient method for the detection and capture of fusion proteins with the FLAG® peptide sequence. ANTI-FLAG M2 Magnetic Beads were validated in https://www.sigmaldrich.com/catalog/product/sigma/m8823?lang=zh&region=CN.</p> <p>3. anti-FLAG (Sigma, Cat# A8592) was validated in Qi et al., 2017 Plant Cell.</p> <p>4. anti-FLAG (Ab-mart, Cat#M20008L, Lot#304585) antibody was validated in http://www.ab-mart.com.cn/</p>

upload/20170614093631xz.pdf

5. Anti-HA-Agarose antibody is the immunoglobulin fraction of Monoclonal Anti-HA (mouse IgG1 isotype) covalently linked to agarose. It is suitable for immunoprecipitation detection and immunoaffinity purification of HA labeled fusion protein. Anti-HA-Agarose antibody was validated in Qi et al., 2017 Plant Cell.
6. Anti-HA antibody (Sigma, Cat#H6533) was validated in Qi et al., 2017 Plant Cell.
7. Anti-GFP (KT Health, Cat# KTS1301) was validated in <http://www.ksm-life.com/cn/product-detail-260.html>.
8. anti-H3 (Histone-H3 Rabbit Polyclonal antibody) was validated in <http://www.ptgcn.com/products/Histone-H3-Antibody-17168-1-AP.htm>

ChIP-seq

Data deposition

- Confirm that both raw and final processed data have been deposited in a public database such as [GEO](#).
- Confirm that you have deposited or provided access to graph files (e.g. BED files) for the called peaks.

Data access links

May remain private before publication.

<https://www.ncbi.nlm.nih.gov/geo/query/acc.cgi?acc=GSE142369>

Files in database submission

GSM4233033 BRM-GFP-Input
 GSM4233034 BRM-GFP-IP-bio1
 GSM4233035 BRM-GFP-IP-bio2
 GSM4233036 brip1brip2 BRM-GFP-Input
 GSM4233037 brip1brip2 BRM-GFP-IP-bio1
 GSM4233038 brip1brip2 BRM-GFP-IP-bio2
 GSM4233039 BRIP1-GFP-Input
 GSM4233040 BRIP1-GFP-IP-bio1
 GSM4233041 BRIP1-GFP-IP-bio2
 GSM4233042 BRIP2-GFP-Input
 GSM4233043 BRIP2-GFP-IP-bio1
 GSM4233044 BRIP2-GFP-IP-bio2
 GSM4487485 brm-1_BRIP1-GFP-Input
 GSM4487486 brm-1_BRIP1-GFP-IP-bio1
 GSM4487487 brm-1_BRIP1-GFP-IP-bio2
 GSM4487488 brm-1_BRIP2-GFP-Input
 GSM4487489 brm-1_BRIP2-GFP-IP-bio1
 GSM4487490 brm-1_BRIP2-GFP-IP-bio2

Genome browser session (e.g. [UCSC](#))

<http://www.igv.org/> (IGV_Win_2.4.14)

Methodology

Replicates

Two biological replicates

Sequencing depth

This information can be found in Supplementary Table 3

Antibodies

anti-GFP, Abcam, Cat#ab290, Lot#GR3196305-1

Peak calling parameters

MACS2 was used for peak calling using the following parameters: Paired-end; Effective genome size=119,667,750; nomodel; extension size=200; q value=0.01.

Data quality

For ChIP-seq, FDR 5%; (See method in the manuscript for details)

Software

ChIP-seq analysis: Bowtie for Illumina version 1.1.2, SAMTools version 3.3.0.0.0, MACS2 version 1.1.2, DeepTools version 2, Integrative Genomics Viewer (version 2.4.14), ChipSeeker Version 1.18.0+galaxy1, DiffBind version 2.10.0
 GO analysis: Metascape